



The Warburg Micro Syndrome-associated Rab3GAP-Rab18 module promotes autolysosome maturation through the Vps34 Complex I

Szabolcs Takáts^{1,2,*} , Luca Lévy¹, Attila Boda¹, Sarolta Tóth¹, Zsófia Simon-Vecsei¹, András Rubics¹, Ágnes Varga¹, Mónika Lippai¹, Péter Lőrincz^{1,2}, Gábor Glatz¹ and Gábor Juhász^{1,3} 

1 Department of Anatomy, Cell and Developmental Biology, ELTE Eötvös Loránd University, Budapest, Hungary

2 Premium Postdoctorate Research Program, Hungarian Academy of Sciences, Budapest, Hungary

3 Institute of Genetics, Biological Research Centre of the Hungarian Academy of Sciences, Szeged, Hungary

Keywords

autophagy; Rab18; Rab3GAP1; Rab3GAP2; Vps34 Complex I

Correspondence

S. Takáts and G. Juhász, Department of Anatomy, Cell and Developmental Biology, ELTE Eötvös Loránd University, Budapest H-1117, Hungary
Tel: +47 22 78 19 35 (ST); +36 1 3722500, ext. 8639 (GJ)
E-mails: szabolcs.takats@rr-research.no (ST); szmrt@elte.hu (GJ)

Present address

*Department of Molecular Cell Biology, Institute for Cancer Research, Oslo University Hospital, Oslo, N-0379, Norway

(Received 15 September 2019, revised 10 February 2020, accepted 26 March 2020)

doi:10.1111/febs.15313

Warburg micro syndrome (WMS) is a hereditary autosomal neuromuscular disorder in humans caused by mutations in Rab18, Rab3GAP1, or Rab3GAP2 genes. Rab3GAP1/2 forms a heterodimeric complex, which acts as a guanosine nucleotide exchange factor and activates Rab18. Although the genetic causes of WMS are known, it is still unclear whether loss of the Rab3GAP-Rab18 module affects neuronal or muscle cell physiology or both, and how. In this work, we characterize a Rab3GAP2 mutant *Drosophila* line to establish a novel animal model for WMS. Similarly to symptoms of WMS, loss of Rab3GAP2 leads to highly decreased motility in *Drosophila* that becomes more serious with age. We demonstrate that these mutant flies are defective for autophagic degradation in multiple tissues including fat cells and muscles. Loss of Rab3GAP-Rab18 module members leads to perturbed autolysosome morphology due to destabilization of Rab7-positive autophagosomal and late endosomal compartments and perturbation of lysosomal biosynthetic transport. Importantly, overexpression of UVRAG or loss of Atg14, two alternative subunits of the Vps34/PI3K (vacuole protein sorting 34/phosphatidylinositol 3-kinase) complexes in fat cells, mimics the autophagic phenotype of Rab3GAP-Rab18 module loss. We find that GTP-bound Rab18 binds to Atg6/Beclin1, a permanent subunit of Vps34 complexes. Finally, we show that Rab3GAP2 and Rab18 are present on autophagosomal and autolysosomal membranes and colocalize with Vps34 Complex I subunits. Our data suggest that the Rab3GAP-Rab18 module regulates autolysosomal maturation through its interaction with the Vps34 Complex I, and perturbed autophagy due to loss of the Rab3GAP-Rab18 module may contribute to the development of WMS.

Introduction

Warburg micro syndrome (hereafter WMS) and Mart-solf syndrome are severe and milder forms of the same hereditary neuromuscular disorder, respectively. Patients suffer from motor disorders, spastic

paraplegia, cataract, and mental retardation [1,2]. Both syndromes are caused by homozygous loss-of-function mutations affecting one of the RAB18, RAB3GAP1, RAB3GAP2, or TBC1D20 genes [3,4]. Although

Abbreviations

Atg, autophagy-related gene; GAP, GTPase-activating protein; GEF, guanosine nucleotide exchange factor; LTR, LysoTracker Red; PI3P, phosphatidylinositol 3-phosphate; Rab, Ras homolog in brain; Syx17, syntaxin 17; UVRAG, UV radiation resistance-associated gene; Vps, vacuole protein sorting; WMS, Warburg micro syndrome.

dozens of disease-causing mutations were identified in these genes [3], how these lead to the onset of WMS is still poorly understood.

Rab18 is a member of the Rab GTPase family proteins, which are the main regulators of endomembrane trafficking. Rabs are switch-like proteins: They bind or release their effector proteins (tethers, motor adaptors, kinases) in their GTP- or GDP-bound states, respectively. The switch between GTP and GDP depends on specific regulatory proteins: guanine nucleotide exchange factors (GEFs) and GTPase-activating proteins (GAPs). GEFs promote the exchange of GDP for GTP; hence, they activate a given Rab. In contrast, GAPs promote GTPase activity and inactivation of their partner Rabs [5]. The activating GEF for Rab18 is the heterodimer Rab3GAP complex, which consists of the catalytic Rab3GAP1 and noncatalytic Rab3GAP2 subunits. The Rab3GAP complex acts as a bivalent Rab regulator: In addition to its GEF function toward Rab18, it also serves as a GAP for Rab3 [6]. As WMS-associated Rab3 mutations have not been identified yet, the onset of WMS in Rab3GAP mutant patients is most likely due to the loss of Rab18 GEF function. Rab18 was found to localize to the ER and lipid droplets [7,8], but some studies showed that Rab18 is also present on the Golgi apparatus [9] and on endosomes [10]. Although it was previously demonstrated that Rab18 is involved in ER-lipid droplet tethering, regulation of lipid droplet dynamics [8,11], and replication of various viruses [12,13], there is no clear evidence for the involvement of these processes in the occurrence of WMS. As both Rab18 and Rab3GAP are regulators of endomembrane trafficking, it seems possible that a certain vesicle transport route is impaired in WMS patients.

Autophagy is an evolutionarily conserved catabolic pathway of eukaryotic cells during which cells degrade aged, superfluous or damaged proteins or organelles through the lysosomal pathway. During the process of macroautophagy (hereafter autophagy), a specific membrane cistern called phagophore emerges in the cytoplasm; then, by sealing of its edges it engulfs cytoplasmic material into a double-membrane vesicle called autophagosome. Autophagosomes eventually fuse with lysosomes and give rise to autolysosomes in which the cargo gets degraded and the resulting organic monomers are released to fuel energy-producing or anabolic pathways [14]. As a recycling and self-renewal process, autophagy contributes to maintaining the health of terminally differentiated cells (such as neurons or muscle fibers) and serves as an important general response to stress (e.g., starvation, presence of oxidative agents) in all

cell types. Perturbation of autophagy, among others, can contribute to cancer, impaired immunity, and early aging [14,15]. Additionally, there is a large body of evidence that flies, mice, and humans defective for autophagy suffer from neuromuscular disorders and progressive neurodegeneration [16–18].

The autophagic pathway converges with endocytosis (the other main lysosomal degradative pathway) at the level of lysosomes, and several Rab proteins are known to regulate both processes. Others and we recently demonstrated that autophagosome–lysosome fusion is promoted by Rab2 and Rab7 [19–23]. While early endosomal Rab5 also enhances autolysosomal degradation, it regulates this process via promoting lysosomal maturation through regulating the phosphatidylinositol 3-phosphate (PI3P) content of endosomal membranes.

Phosphatidylinositol 3-phosphate is produced by the class III phosphatidylinositol 3-kinase (PI3K) complex. The core of the complex consists of three permanent subunits: the catalytic Vps34 lipid kinase and the two regulatory subunits, Vps15 and Atg6. The core complex can bind one from the two alternative and mutually exclusive subunits, Atg14 or UVRAG, which regulate its activity and organelle specificity. The complex consisting of the heterotrimeric core and Atg14 is also known as Vps34 Complex I, and it is considered to promote autophagosome formation. In contrast, the Vps34 Complex II that contains the heterotrimeric core and UVRAG produces PI3P on endosomes and promotes their maturation to late endosomes and lysosomes [19,24]. It is important to note that further facultative subunits have been described in addition to Atg14 and UVRAG such as Atg38/NRBF2 [25]. Since their activity is still dependent on the presence of Atg14 or UVRAG, they do not define a new Vps34 complex type [26]. Hereafter, we simply refer to the Atg14- or UVRAG-containing heterotetramers as Vps34 Complex I or Vps34 Complex II, respectively. The Vps34 Complex II acts as a Rab5 effector on endosomal membranes [5,19], while emerging evidence suggests that the autophagosomal activity of Complex I is independent of Rab5 [19,24,27]. However, we cannot rule out the possibility that Complex I acts as an effector of another Rab protein.

Although a few previous studies suggested that loss of Rab18 or the Rab3GAP complex influences autophagy [28,29], their precise role in the regulation of this process and whether it can be connected to WMS is still poorly understood. In this study, we establish a new Rab3GAP2-deficient *Drosophila* model for WMS and demonstrate that Rab3GAP-Rab18 module, through its interaction with the Vps34 Complex I,

regulates autophagy by promoting the maturation of lysosomes/autolysosomes.

Results

Aged Rab3GAP2 mutant flies show neuromuscular and autophagy defects

To establish a novel animal model of WMS, we utilized the Rab3GAP2[MI11001] (hereafter Rab3GAP [MI]) mutant *Drosophila* line. This line carries a Minos transposable element insertion in the third exon of the eight exon-containing Rab-3gap/CG7061 (hereafter Rab3GAP2) gene at the 1438th nucleotide from the transcription start site, disrupting the protein-coding sequence after amino acid H434; thus, we considered it as a potentially strong loss-of-function allele. To test whether these flies show motility defects similarly to WMS patients, we performed climbing assays, a well-established method for investigating the neuromuscular function of adult *Drosophila*. We observed that young, 8-day-old Rab3GAP2 mutants climbed significantly slower than controls did (Fig. 1A,B). This difference became more severe when we repeated the test on the same cohorts of flies on the 32th day after their eclosion. Although the motility of control flies also decreased by age, the old Rab3GAP2 mutants showed critically low motility: They were almost unable to climb (Fig. 1A,B). This motility defect highlights that Rab3GAP2 mutant *Drosophila* can be a useful animal model for understanding WMS.

Age-dependent loss of neuromuscular function is a well-known hallmark of defective autophagy [16]. To investigate whether the autophagic flux is intact in Rab3GAP2 mutants, we measured levels of the selective autophagic cargo p62 and the autophagic membrane-associated, lipid-conjugated form of Atg8a (Atg8a II) by western blot. To assay neuronal and muscular tissues separately, we collected samples from heads (containing mostly the brain and hardly any muscles) versus bodies (lots of muscles and no nervous tissue) of 30-day-old control and Rab3GAP2[MI] hemizygous flies. Interestingly, we observed no striking differences between the level of autophagy markers of control and Rab3GAP2 mutant head samples (Fig. 1C). In contrast, Rab3GAP2 mutant bodies showed increased levels of p62 and Atg8a II compared with the controls. The high levels of autophagy markers were further elevated in mutants following autophagy induction by 3 h of starvation (Fig. 1C). The accumulation of these specific autophagic cargos in Rab3GAP2-deficient samples indicates that the autophagic degradation is severely compromised in certain

tissues, including probably the muscles of Rab3GAP2 mutant flies. To test the autophagic activity directly in muscles, we performed anti-Atg8a and anti-p62 immunostainings on muscle tissue of 30-day-old control and Rab3GAP2 mutant flies. We observed that the Rab3GAP2-deficient thoracic muscles accumulated large p62 aggregates that were also positive for Atg8a (Fig. 1D–F). These findings suggest that defective autophagy in muscle cells may contribute to the poor climbing ability of Rab3GAP2 mutant flies and highlight the important, but yet unclear function of Rab3GAP2 in autophagy.

Rab3GAP-Rab18 module members regulate the same step of the autophagic process

To understand the role of Rab3GAP2 in autophagy, we turned to a popular autophagy model system, the fat tissue of L3 larvae. In well-fed larvae, autophagy occurs at a very low basal level; however, even a short starvation of early L3 stage larvae is able to induce extreme high levels of autophagy in this tissue. To elucidate which step of the autophagic process is perturbed in Rab3GAP2 loss-of-function cells, we investigated fat tissues from starved control and Rab3GAP2 mutant larvae, by using the mCherry-Atg8a reporter to label autophagic structures: phagophores, autophagosomes, and autolysosomes. Upon 3 h of starvation, bright, round-shaped mCherry-Atg8a-positive autophagic structures appeared in the control cells (Fig. 2A,C). In contrast, this punctate morphology was seriously disturbed in Rab3GAP2 mutant fat cells: The autophagic compartment showed a perinuclear, network-like pattern (Fig. 2B,C). This ‘autophagic network’ contained elongated chain-like structures composed of small interconnected puncta and single tubules.

Based on our results from adult flies, we hypothesized that the onset of WMS in Rab3GAP-Rab18 module mutant patients may be facilitated by an autophagy defect. To further understand the underlying molecular causes of this disorder, we aimed to investigate the knockdown phenotypes of Rab18, CG31935 (the *Drosophila* ortholog of Rab3GAP1, hereafter called Rab3GAP1), and Rab3GAP2 genes by targeting them with two independent RNAi lines. For these experiments, we utilized the so-called Flp-FRT technique using the *hsp70-Flp* and *Act-FRT-CD2-FRT-Gal4* genetic elements [30] to generate GFP-positive knockdown cell clones in fat tissue of starved L3 larvae. Silencing of any Rab3GAP-Rab18 genes in GFP-positive cell clones resulted in the appearance of the perinuclear network of chain-like mCherry-Atg8a-

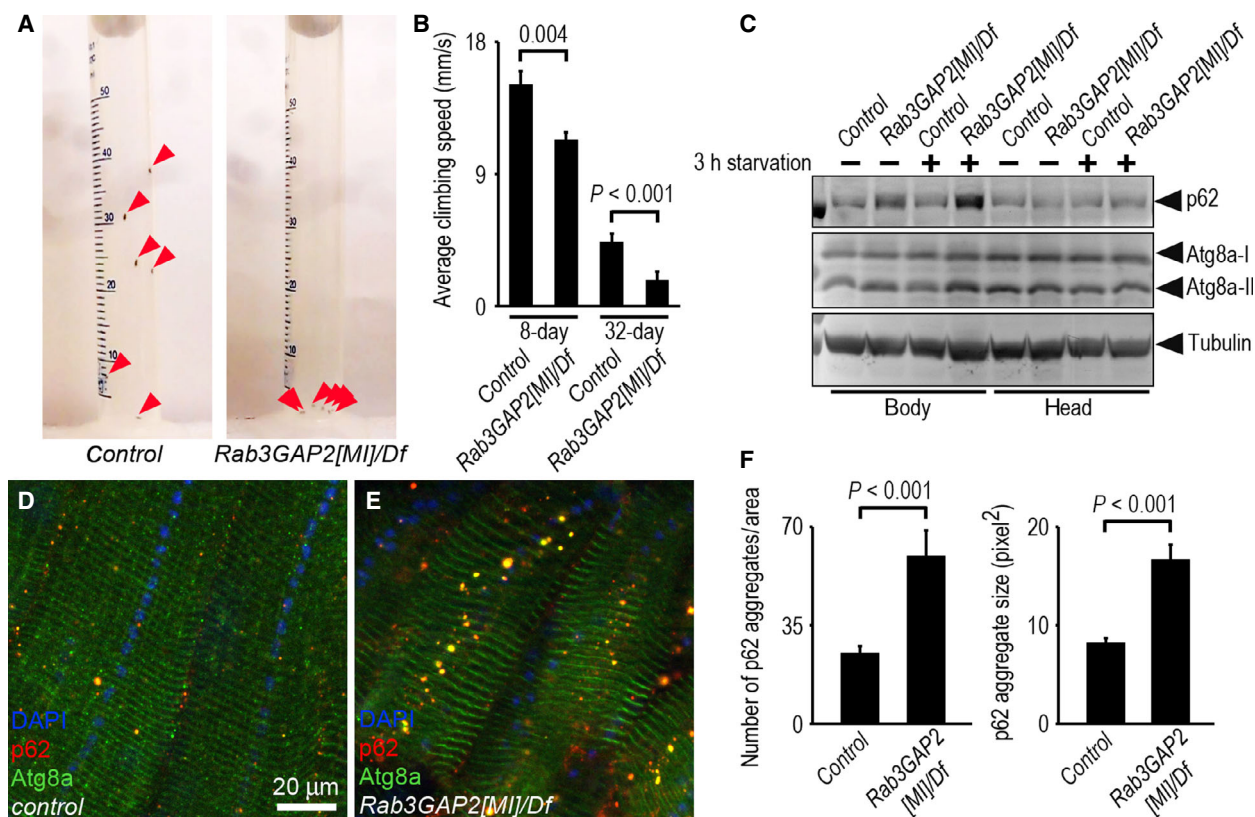


Fig. 1. Aged Rab3GAP2 mutant flies show ataxia and impaired autophagy in muscles. (A) Representative images of the climbing status of 32-day-old control and Rab3GAP2 mutant flies (arrowheads) after 5 s of climbing. (B) Quantification of the climbing data from experiments with 8- and 32-day-old flies, data represented as the mean, error bars show the standard error, Mann–Whitney tests, $n = 30$ /genotype. (C) Autophagy cargos p62 and Atg8a-II accumulate in body (thorax and abdomen) but not in head lysates from 30-day-old Rab3GAP2 mutant flies kept in fed conditions or exposed to 3 h of starvation. (D, E) Large p62 and Atg8a double-positive aggregates appear in thoracic muscles of 30-day-old Rab3GAP2 mutant (E) but not in control (D) flies. (F) Quantification of data from D and E, data represented as the mean, error bars show the standard error, Mann–Whitney and two-tailed, two-sample t -test for number and size, respectively, $n = 10$. Scale bar in D is the same for E. Experiments shown on A–C and D, E were done twice and three times, respectively, and representative data are shown.

positive structures and tubules (Fig. 2D–J), reminiscent of the phenotype that we observed in Rab3GAP2 mutant cells (Fig. 2B,C). These data indicate that the Rab3GAP-Rab18 module members regulate the same step of the autophagic process.

To understand whether Rab3GAP2 regulates both basal autophagy and starvation-induced autophagy, we performed anti-p62 western blot experiments on lysates of well-fed and starved early L3 stage larvae. This experiment showed that in both fed and starved conditions, Rab3GAP2[M] hemizygous larvae accumulate p62 compared with controls; this buildup of p62 could be rescued by endogenous promoter-driven expression of a wild-type Rab3GAP2 transgene in mutants (Fig. 2K). This finding indicates that loss of Rab3GAP2 impairs both basal and starvation-induced autophagic degradation.

Loss of the Rab3GAP-Rab18 module perturbs autolysosome morphology

We carried out additional confocal microscopy experiments to elucidate the identity of the unusual chain-like mCherry-Atg8a structures in these mutants. We generated GFP-marked Rab3GAP2[M] homozygous mutant fat cell clones, and we stained the fat tissue of starved L3 larvae with LysoTracker Red (LTR). This acidophilic vital dye labels autolysosomes as bright round-shaped red puncta in GFP-negative control cells (Fig. 3A,J). In contrast, in GFP-positive mutant clones, we observed a perinuclear network of elongated, chain-like acidic structures (Fig. 3A,J). Additionally, RNAi-mediated knockdown of Rab3GAP-Rab18 module genes resulted in the same abnormal autolysosome morphology (Fig. 3B–D,J). In a parallel

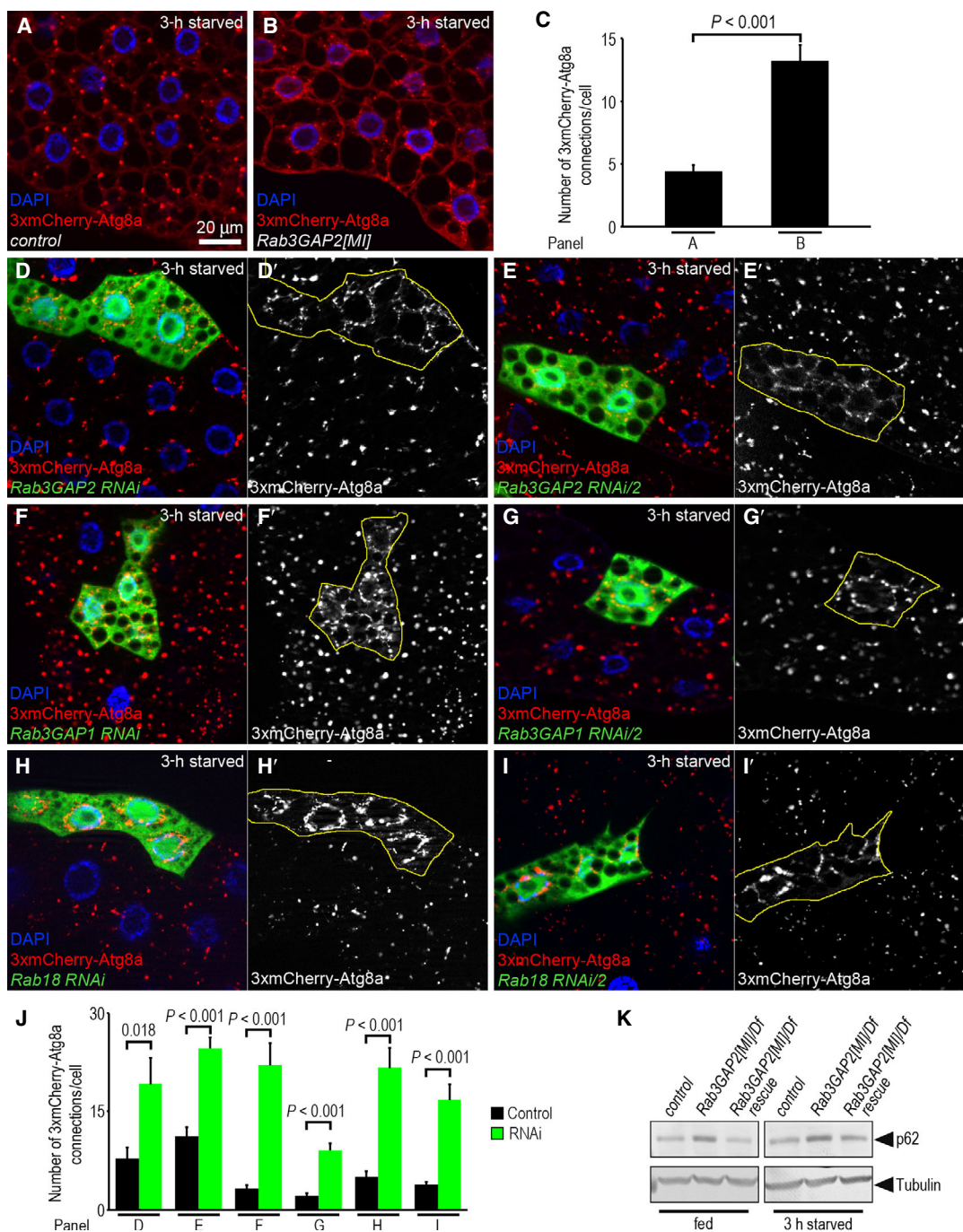


Fig. 2. Loss of Rab3GAP-Rab18 module function perturbs the morphology of autophagic structures. (A) The mCherry-Atg8a reporter shows large punctate autophagic structures in fat cells of control starved larvae. (B) Perinuclear network of elongated, chain-like mCherry-Atg8a-positive structures is visible in Rab3GAP2[M/I] homozygous fat tissue. (C) Quantification of data from A and B, data represented as the mean, error bars show the standard error, two-tailed, two-sample *t*-test, *n* = 10. (D–I) Chain-like mCherry-Atg8a-positive autophagic structures appear in GFP-positive Rab3GAP2 (D, E), Rab3GAP1 (F, G), or Rab18 (H, I) RNAi fat cells compared with the surrounding GFP-negative control cells, which contain mostly large round autolysosomes. (J) Quantification of data from D–I, data represented as the mean, error bars show the standard error, two-tailed, two-sample *t*-test for D–G and Mann–Whitney test for H, I, *n* = 10. (K) The autophagic cargo p62 accumulates in lysates of fed and starved Rab3GAP2 mutants but not in control or Rab3GAP2-rescued larvae. Scale bar in A is the same for B, D–I. RNAi-silenced clone cells are encircled by yellow in D'–I'. Experiments shown on A, B, and D–I, K were done twice and three times, respectively, and representative data are shown.

experiment, we further investigated the lysosome/autolysosome compartment by using the common lysosomal membrane reporter Lamp-mCherry [19]. We observed the same phenotypes as previously: This marker showed punctate pattern in the control (Fig. 3E) and aberrant, perinuclear network of chain-like lysosomes in the Rab3GAP2 mutant fat cells and Rab3GAP1/2 or Rab18 RNAi clones (Fig. 3F–I,K,L). These findings indicate that the aberrant network of autophagic structures observed in Rab3GAP-Rab18 loss-of-function cells is composed of aberrant autolysosomes.

One could suppose that impaired autolysosome morphology can be a consequence of attenuated autophagosome–lysosome fusion in Rab3GAP-Rab18 module loss-of-function cells. To test this hypothesis, we performed immunolabeling experiments to assay the colocalization rate of the autophagy marker mCherry-Atg8a and the lysosomal-resident GTPase Arl8 in control and Rab3GAP2 mutant cells. In control cells, we observed that the vast majority (85.83%, $n = 120$) of autophagic structures are also positive for the lysosomal marker (Fig. 4A). In contrast, we found a moderate decrease in the overlap between these two markers (66.67%, $n = 120$) in cells homozygous for Rab3GAP2 mutation (Fig. 4B). Compared to the control cells (81.67%, $n = 120$), we also observed a reduced colocalization rate between the mCherry-Atg8a autophagic and the GFP-Lamp1 lysosomal reporters in clones silencing Rab3GAP2 (56.67%, $n = 120$), Rab3GAP1 (63.33%, $n = 120$), or Rab18 (40.83%, $n = 120$) (Fig. 4C–F). Considering that this decrease was moderate and mCherry-Atg8a and Arl8 or GFP-Lamp1 double-positive structures were still present in large numbers, we concluded that autophagosome–lysosome fusion may only be partially impaired in Rab3GAP-Rab18 loss-of-function cells.

This result was further confirmed by ultrastructural analysis. Unlike the large and evenly distributed autolysosomes seen in wild-type cells, Rab3GAP2[M]

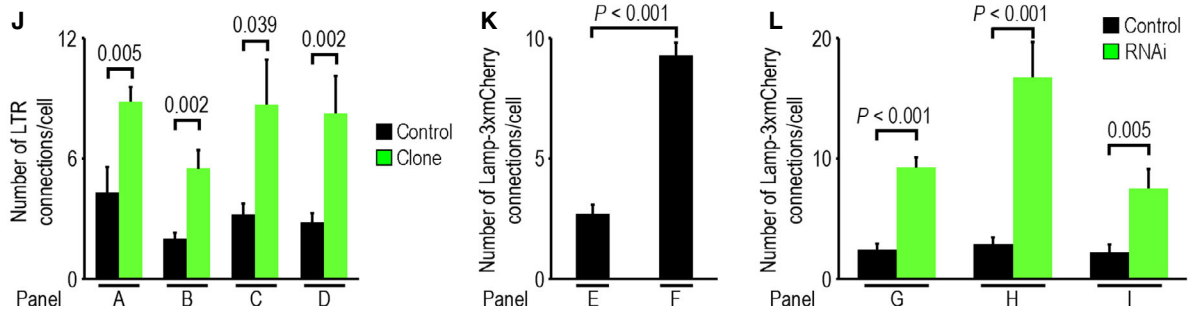
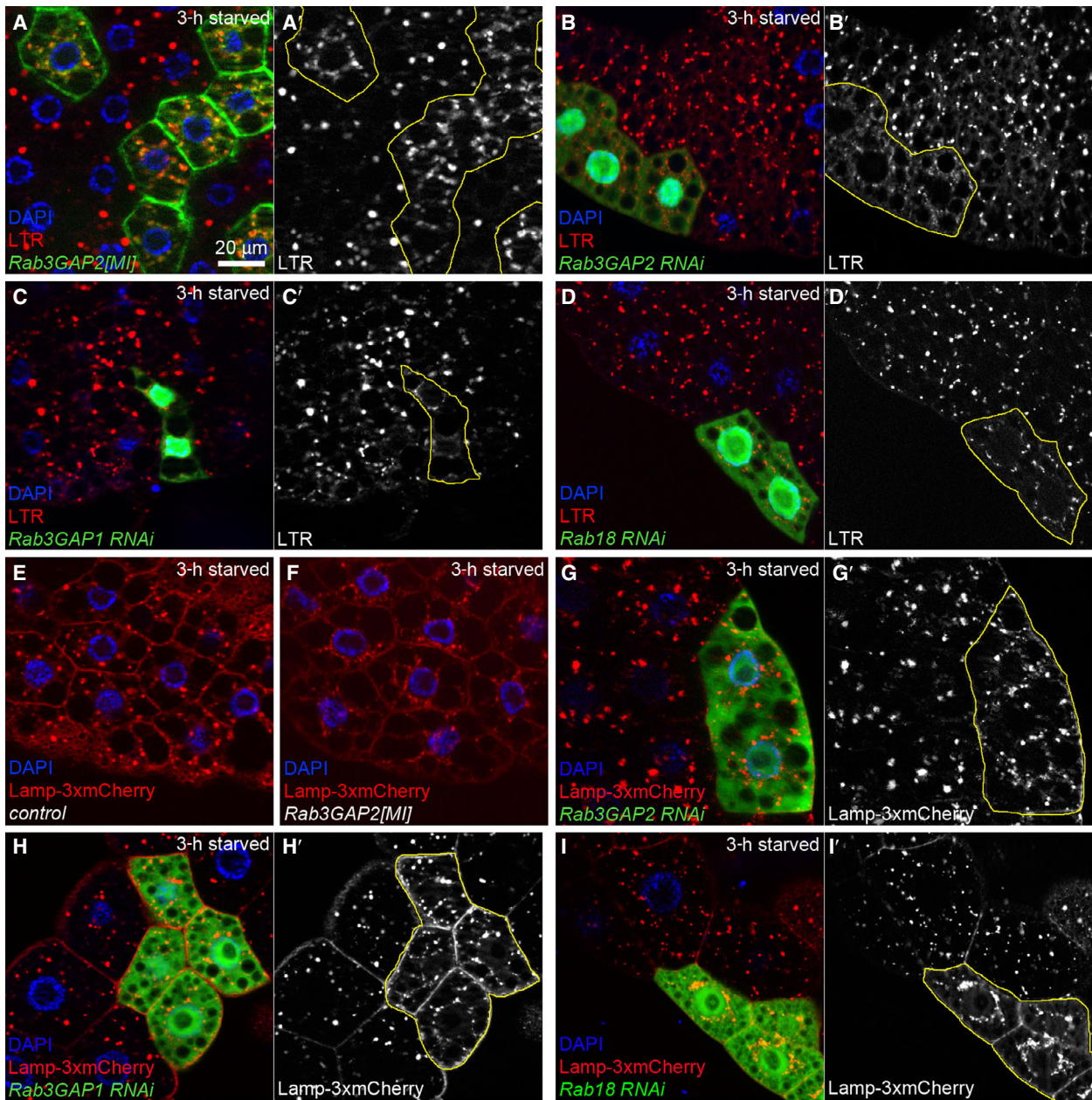
hemizygous mutant fat cells contained small autolysosomes showing unusual, chain-like/clustered distribution, and these were interconnected by simple connecting points or longer ‘bridge-like’ structures (Fig. 5A,B). We also observed clusters of unfused autophagosomes in these mutant cells, which may be the result of a less-efficient autophagosome–lysosome fusion. As these autolysosome ‘chains’ obviously contained cytoplasm-derived material, loss of Rab3GAP-Rab18 module function likely results in defective autolysosome morphology and impaired degradation without playing a major role in autophagosomal fusion events.

We also aimed to visualize the 3D structure of the lysosome chains. Thus, we performed high-magnification laser scanning confocal microscopy on Lamp-mCherry-expressing Rab3GAP1 RNAi clones and acquired Z-stack images (Fig. 5C). After 3D rendering of the Z-stack slices, we generated a video, which clearly demonstrates the 3D structure of lysosome chains (Fig. 5C, Video S1).

The Rab3GAP-Rab18 module is important for proper lysosomal maturation

Perturbed autolysosomal morphology and degradation could be a sign of a general lysosome maturation defect in Rab3GAP-Rab18 module-deficient cells. Lysosome maturation is highly dependent on the integrity of early and late endosomal compartments as well as on sufficient biosynthetic transport to lysosomes. Thus, we investigated the morphology of early and late endosomal and lysosomal compartments in Rab3GAP2 mutant fat cell clones. By immunostaining of the early endosomal protein Rab5 in fat tissue of starved *Drosophila* larvae, we observed that most of the early endosomes localized to the cell periphery, in addition to a small perinuclear cohort of Rab5-positive vesicles. This Rab5 pattern was similar in control cells and Rab3GAP2 mutant clones (Fig. 6A,B).

Fig. 3. Rab3GAP2 regulates autolysosome morphology (A–D) LTR-positive lysosomal/autolysosomal compartment shows defective, elongated, and highly interconnected, network-like morphology in GFP-positive Rab3GAP2 (A) mutant or Rab3GAP2 (B), Rab3GAP1 (C), and Rab18 RNAi (D) fat cell clones compared with the surrounding GFP-negative control cells. (E, F) Punctate lysosomal Lamp-3xmCherry pattern visible in control (E) fat cells is highly perturbed in Rab3GAP2 mutant (F) tissue and shows a perinuclear network of chain-like structures. (G–I) Knockdown of Rab3GAP2 (G), Rab3GAP1 (H), and Rab18 (I) genes in GFP-positive clones results in impaired, network-like Lamp-3xmCherry morphology. (J) Quantification of data from panels A–D, data represented as the mean, error bars show the standard error, Mann–Whitney test for A, B, and D and two-tailed, two-sample *t*-test for C, $n = 10$. (K) Quantification of data from panels E and F, data represented as the mean, error bars show the standard error, two-tailed, two-sample *t*-test, $n = 10$. (L) Quantification of data from panels G–I, data represented as the mean, error bars show the standard error, Mann–Whitney tests, $n = 10$. Scale bar in A is the same for B–I. Mutant and RNAi-silenced clone cells are encircled by yellow in A’–D’ and G’–I’. All experiments were done twice, and representative data are shown.



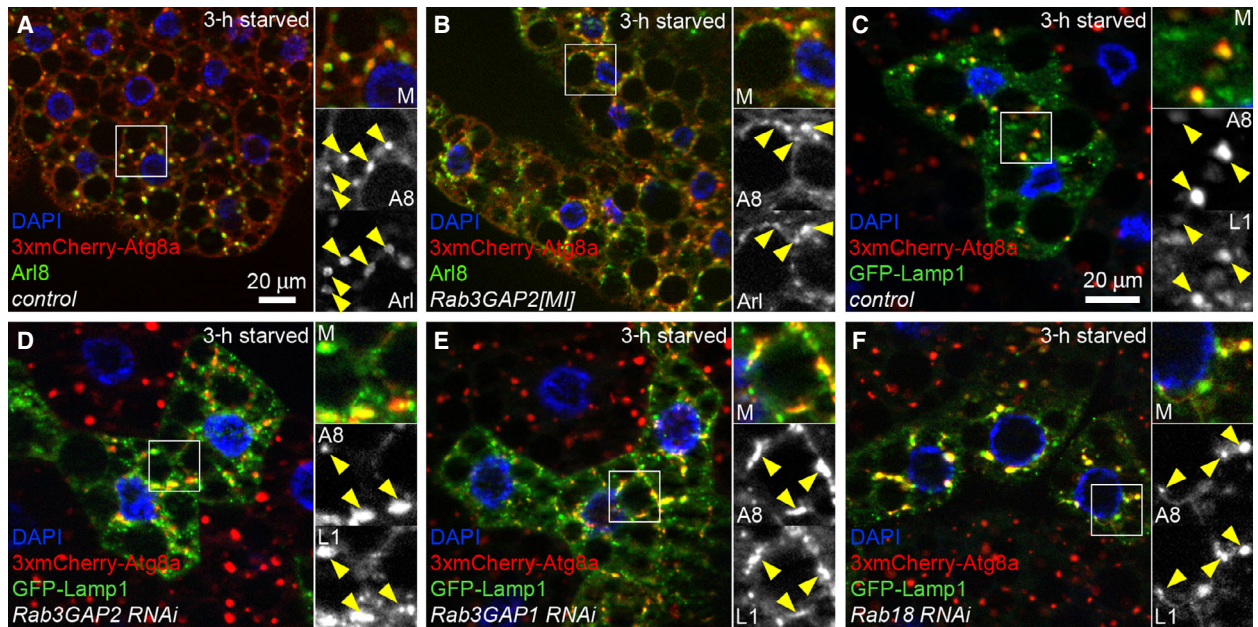


Fig. 4. Loss of Rab3GAP-Rab18 module has a minor effect on autophagosome–lysosome fusion. (A) After 3 h of starvation, autophagic 3xmCherry-Atg8a extensively colocalizes with the lysosome marker Arl8 on punctate structures in control fat cells. (B) This colocalization is somewhat reduced but still obvious in Rab3GAP2 mutant tissue. (C–F) 3xmCherry-Atg8a and the lysosomal GFP-Lamp1 reporters colocalize both in control (C) and, to a lesser extent, in Rab3GAP2 (D), Rab3GAP1 (E), and Rab18 (F) RNAi cells. Small panels in A–F show enlarged merged and grayscale views of the red and green channels of the boxed areas. Arrowheads indicate colocalizing signals. Scale bar in A and C is the same for B and D–F, respectively. All experiments were done twice, and representative data are shown.

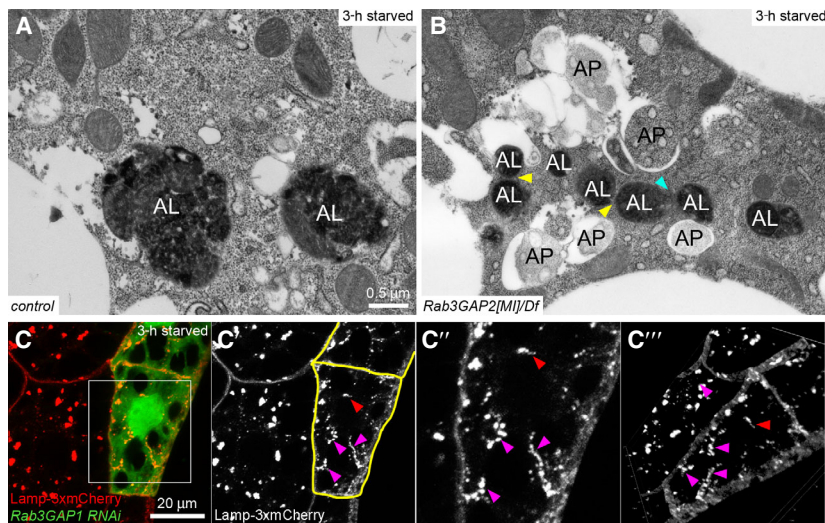


Fig. 5. Autophagosome clusters and lysosome chains accumulate in Rab3GAP2 mutants. (A, B) Large, round-shaped, dense autolysosomes (AL) are visible in EM images from fat cells of starved control larvae (A); in contrast, fat cells from Rab3GAP2 mutants (B) show chain-like autolysosomes connected by simple connecting points (yellow arrowheads) or bridge-like structures (cyan arrowhead) and autophagosome (AP) clusters in EM. (C) High-magnification Z-stack image, compressed from 21 slices (0.1 μm thickness/slice), showing lysosome chains (purple arrowhead) and single tubule (red arrowhead) emanating from a solitary lysosome. C' shows enlarged grayscale view of the red channel of the boxed area from C'. C''' represents a 3D screenshot from Video S1. Scale bar in A is the same for B. RNAi-silenced clone cells are encircled by yellow in C'. All experiments were done twice, and representative data are shown.

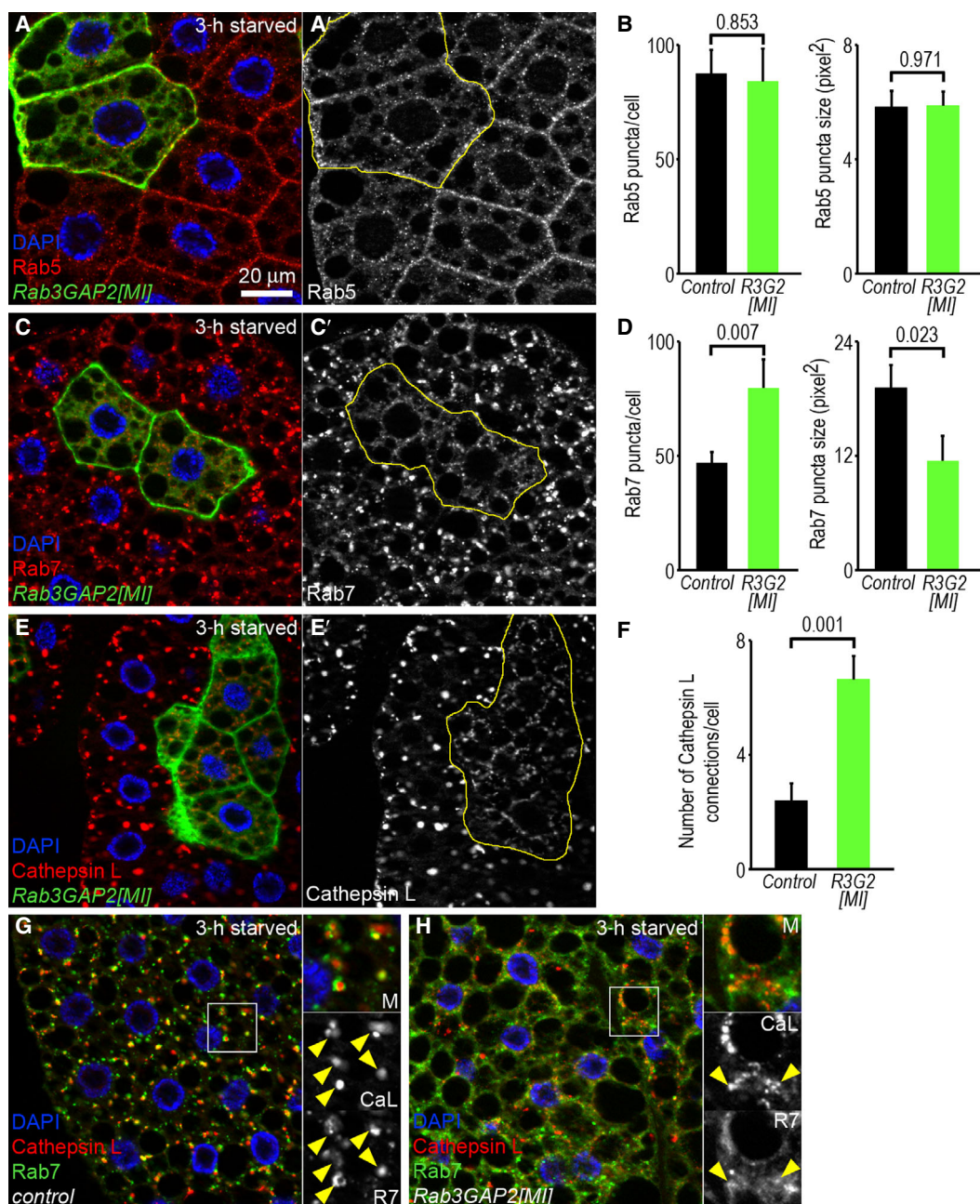


Fig. 6. Rab3GAP2 is required for the maturation of late endosomes and lysosomes. (A) GFP-positive Rab3GAP2 mutant fat cell clones show no defects in the morphology of Rab5-positive early endosomes compared with the GFP-negative control cells. (B) Quantification of data from A, data represented as the mean, error bars show the standard error, two-tailed, two-sample *t*-test for number and Mann–Whitney test for size, $n = 10$. (C) Morphology of the Rab7-positive late endosomal and lysosomal compartment is highly fragmented in GFP-positive Rab3GAP2 mutant clones. (D) Quantification of data from C, data represented as the mean, error bars show the standard error, Mann–Whitney tests, $n = 10$. (E) Cathepsin L-positive lysosomal compartment shows an abnormal, chain-like morphology in GFP-positive Rab3GAP2 mutant cell clones compared with the large, round-shaped lysosomes and autolysosomes that are visible in GFP-negative control cells. (F) Quantification of data from E, data represented as the mean, error bars show the standard error, two-tailed, two-sample *t*-test, $n = 10$. (G, H) The lysosomal hydrolase Cathepsin L localizes to Rab7-positive late endosomes and lysosomes in control fat tissue (G). In contrast, this colocalization is highly reduced in Rab3GAP2 mutants (H). Small panels on G and H show enlarged and merged grayscale views of red and green channels of the boxed areas. Arrowheads indicate colocalizing signals in G and H. Scale bar in A is the same for C, E, G, and H. Rab3GAP2[M] homozygous mutant clone cells are encircled by yellow in A', C', and E'. Experiments shown on A, E, G, H, and C were done twice and three times, respectively, and representative data are shown.

The late endosomal/lysosomal marker Rab7, together with the lysosomal marker Cathepsin L, localized to large punctate or ring-like structures uniformly distributed in the cytoplasm of control cells. In contrast, these structures became fragmented (in case of Rab7) or more chain-like (in case of Cathepsin L) in Rab3GAP2 mutant cells, indicating the striking perturbation of these compartments (Fig. 6C–F). The different phenotypes of Rab7- and Cathepsin L-labeled compartments may be due to the distinct function of the two marker proteins. While Cathepsin L is an acidic hydrolase localized in the lysosomal lumen, Rab7 is a peripheral membrane protein that dynamically associates with and dissociates from the cytoplasmic leaflet of late endosomal/lysosomal membranes and plays a critical role in the maturation of these compartments [31]. Thus, the altered distribution and/or amount of Rab7 can indicate lysosomal maturation defects.

Next, we asked whether the lysosomal biosynthetic pathways, such as the delivery of Cathepsin L, are affected in Rab3GAP2 mutant fat cells. To address this question, we tested the colocalization rate of Cathepsin L and the late endosomal/lysosomal marker Rab7 as double-positive vesicles would represent mature lysosomes/autolysosomes. We found high colocalization (90.67% of Cathepsin L puncta, $n = 150$) in control starved fat cells (Fig. 6G). This was perturbed in Rab3GAP2 mutant cells: The colocalization between these two markers strongly decreased (54% of Cathepsin L puncta, $n = 150$), and separate Rab7 and Cathepsin L vesicles were frequently detected (Fig. 6H). These findings suggest that lysosome maturation is perturbed in cells lacking the Rab3GAP-Rab18 module.

Loss of the Vps34 Complex I resembles the autophagy phenotype of Rab3GAP-Rab18 depletion

As loss of the Rab3GAP-Rab18 module only affected late endosomal and lysosomal but not early endosomal compartments, we hypothesized that it may function in concert with factors known to regulate late endosomal and lysosomal maturation. These processes are highly dependent on the increasing PI3P content of the endosomal membrane [32]. The main source of endosomal PI3P is the Rab5-dependent activity of the Vps34 Complex II [19,27]. In our previous studies, we showed that loss of Rab5 or its effector, the Vps34 Complex II perturbs autolysosomal maturation and degradation; however, none of these mutants showed chain-like autolysosome morphology [19]. The

potential role of Complex I in autolysosome maturation is uncharacterized. Interestingly, a large-scale protein–protein interaction study of *Drosophila* Rab proteins demonstrated that the only Rab found to bind to Atg14 together with other PI3K subunits was Rab18 [33]. This raises the possibility that the Complex I may be the effector through which the Rab3GAP-Rab18 module controls autolysosome maturation.

To understand whether the Vps34 Complex I acts as a Rab18 effector in the course of lysosome/autolysosome maturation, we investigated the morphology of lysosomes in Atg14 loss-of-function fat cells. Knocking down Atg14 by expressing an RNAi transgene resulted in chain-like lysosome morphology based on the pattern of the lysosomal reporter Lamp-mCherry and immunolabeling of the lysosomal GTPase Arl8 [34] (Fig. 7A,C,G,H). Additionally, we also observed a network of chain-like lysosomes in Atg14 mutant cells but not in control fat tissue by Cathepsin L immunostaining (Fig. 7E,F,I).

A previous study demonstrated that overexpressed UVRAG can outcompete Atg14 from the Vps34 complex in human cells [35]. Thus, we hypothesized that cells overexpressing UVRAG may display a phenotype similar to Atg14 loss-of-function cells. To test this, we overexpressed a functional UVRAG transgene in fat cell clones, which resulted in interconnected chain-like Lamp-mCherry and Arl8 patterns (Fig. 7B,D,G,H) similar to what we found in Atg14 knockdown cells. Along the same lines, decreased function of the Vps34 Complex I disturbed the Rab7-positive late endosomal/lysosomal compartment: Both Atg14 loss-of-function and UVRAG-overexpressing cells contained fainter and smaller Rab7-positive structures (Fig. 8A,B,D). Finally, overexpression of UVRAG affected the pattern of mCherry-Atg8a-positive structures similarly to that of Rab3GAP-Rab18 module-depleted cells (Fig. 8C,E).

To further support that loss of Vps34 Complex I perturbs autolysosome morphology, we performed correlative ultrastructural analysis on UVRAG-overexpressing fat cell clones from starved larvae. We observed defectively small autolysosomes arranged to chain-like structures (Fig. 8F), similarly to that we found earlier in Rab3GAP2 mutants (Fig. 5B).

Our findings demonstrate that loss of function of both the Rab3GAP-Rab18 module and the Vps34 Complex I results in very similar lysosome morphology defects and in destabilization of the Rab7-positive compartment, suggesting that these factors act together to promote lysosome/autolysosome maturation.

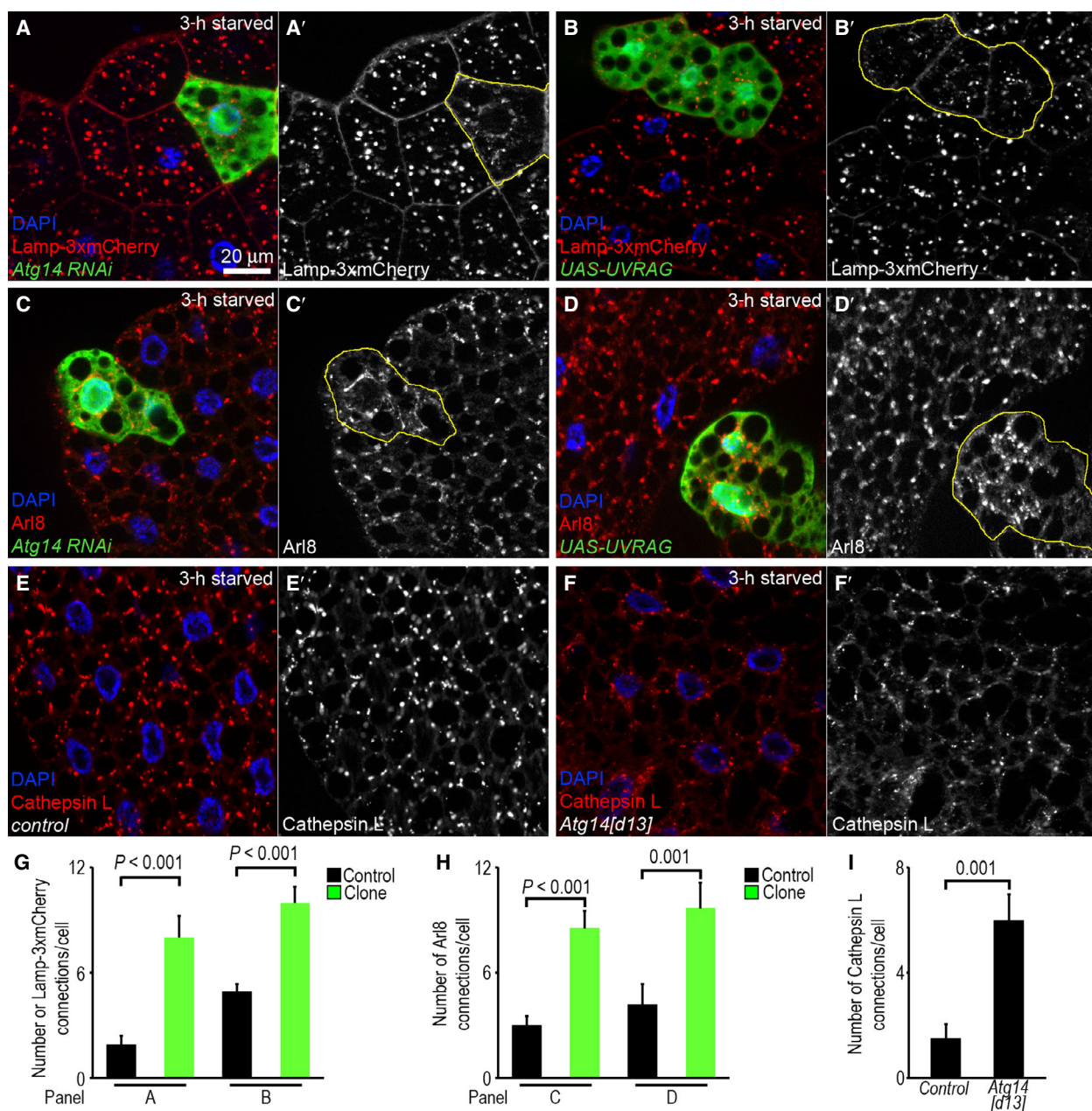


Fig. 7. Loss of Vps34 Complex I function results in perturbed lysosome morphology. (A, B) The increased amount of Lamp-3xmCherry-positive, abnormally shaped, chain-like lysosomes is obvious in GFP-positive Atg14 RNAi (A)- or UVRAG-overexpressing (B) fat cell clones. (C, D) Immunolabeling of the lysosome marker Arl8 indicates the chain-like morphology of the lysosomal compartment in Atg14 RNAi (C)- and UVRAG-overexpressing (D) GFP-positive clones. (E, F) Large round lysosomes are seen in the fat tissue of starved control larvae immunolabeled with anti-Cathepsin L (E). In contrast, Cathepsin L-positive structures appear in chain-like pattern in Atg14 mutant fat cells (F). (G) Quantification of data from A, B, data represented as the mean, error bars show the standard error, Mann-Whitney test for A and two-tailed, two-sample *t*-test for B, $n = 10$. (H) Quantification of data from C, D, data represented as the mean, error bars show the standard error, two-tailed, two-sample *t*-test for C and Mann-Whitney test for D, $n = 10$. (I) Quantification of data from E, F, data represented as the mean, error bars show the standard error, two-tailed, two-sample *t*-test, $n = 10$. Scale bar in A is the same for B–F. RNAi-silenced or transgene-overexpressing clone cells are encircled by yellow in A'–D'. All experiments were done twice, and representative data are shown.

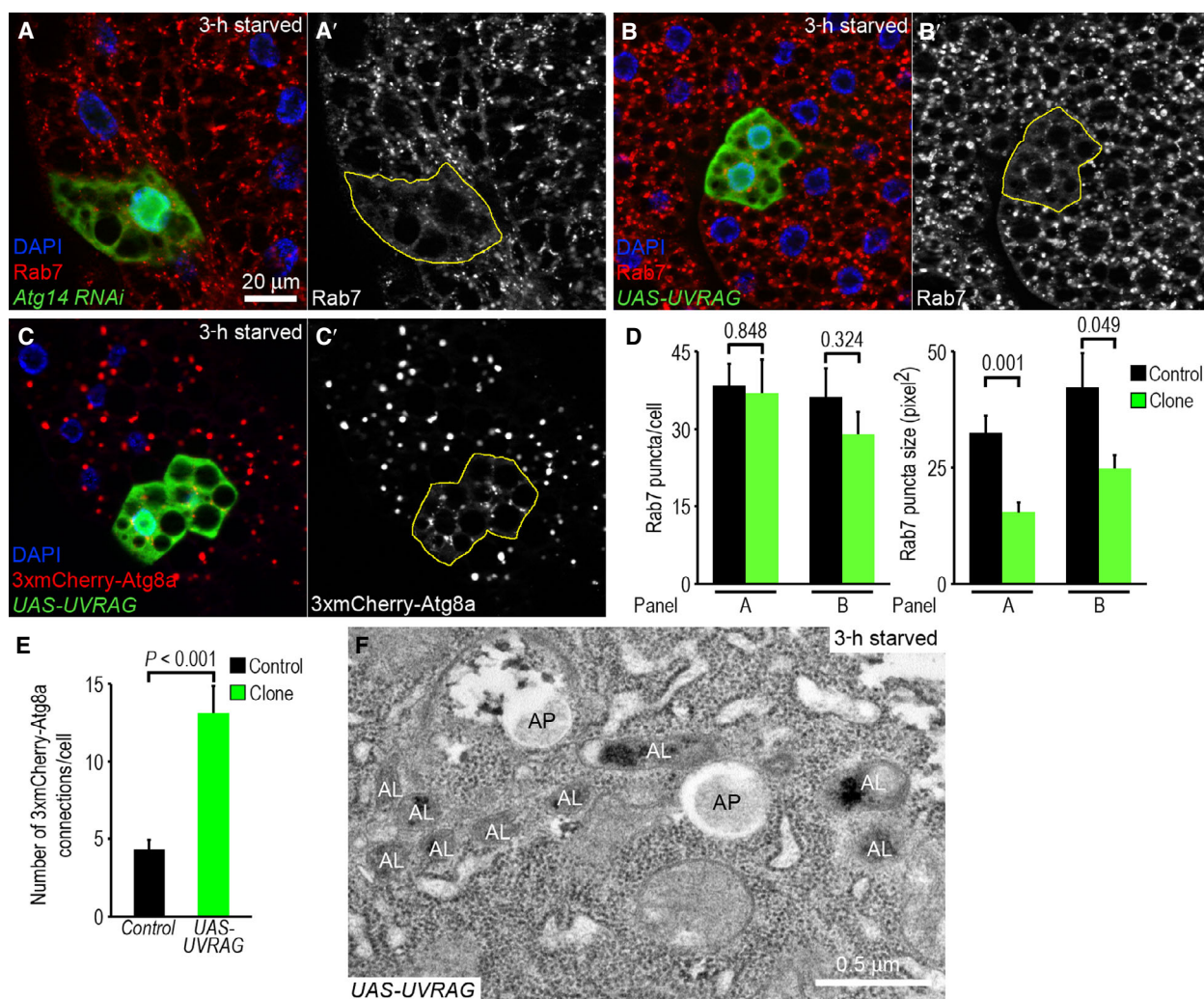


Fig. 8. Rab7-positive compartment is fragmented in cells lacking Vps34 Complex I. (A, B) The late endosome/lysosome marker Rab7 shows a dispersed pattern in GFP-positive Atg14 RNAi (A)- or UVRAG-overexpressing (B) fat cells compared with the surrounding GFP-negative control cells. (C) Overexpression of UVRAG in GFP-positive fat cell clones leads to the appearance of chain-like 3xmCherry-Atg8a-positive autophagic structures. (D) Quantification of data from A and B, data represented as the mean, error bars show the standard error, two-tailed, two-sample *t*-tests, *n* = 10. (E) Quantification of data from C, data represented as the mean, error bars show the standard error, two-tailed, two-sample *t*-test, *n* = 10. (F) Autolysosome (AL) chains and autophagosomes (AP) are visible in the ultrastructural image of an UVRAG-overexpressing fat cell clone. Scale bar in A is the same for B, C. RNAi-silenced or transgene-overexpressing clone cells are encircled by yellow in A'–C'. All experiments were done twice, and representative data are shown.

Vps34 Complex I regulates lysosome maturation as a Rab18 effector

Although the previously mentioned large-scale study demonstrated that Rab18 physically interacts with Vps34 Complex I subunits [33], this interaction was not characterized extensively. To understand which Vps34 Complex I subunits are directly involved in Rab18 binding and whether it depends on the GTP binding status of Rab18, we performed yeast two-hybrid experiments. Importantly, a strong interaction

was observed between Atg6-bound and GTP-bound but not GDP-bound Rab18 (Fig. 9A). Interestingly, none of the other Vps34 Complex I subunits showed direct interaction with Rab18, regardless of its guanine nucleotide-bound state (Fig. 9A). We further confirmed this interaction in GST pull-down experiments using lysates of Atg6-HA larvae. Atg6-HA clearly bound to the GTP-locked mutant form of recombinant GST-Rab18 (Fig. 9B). Since the exclusive binding to their GTP-loaded Rabs is a hallmark of Rab effectors

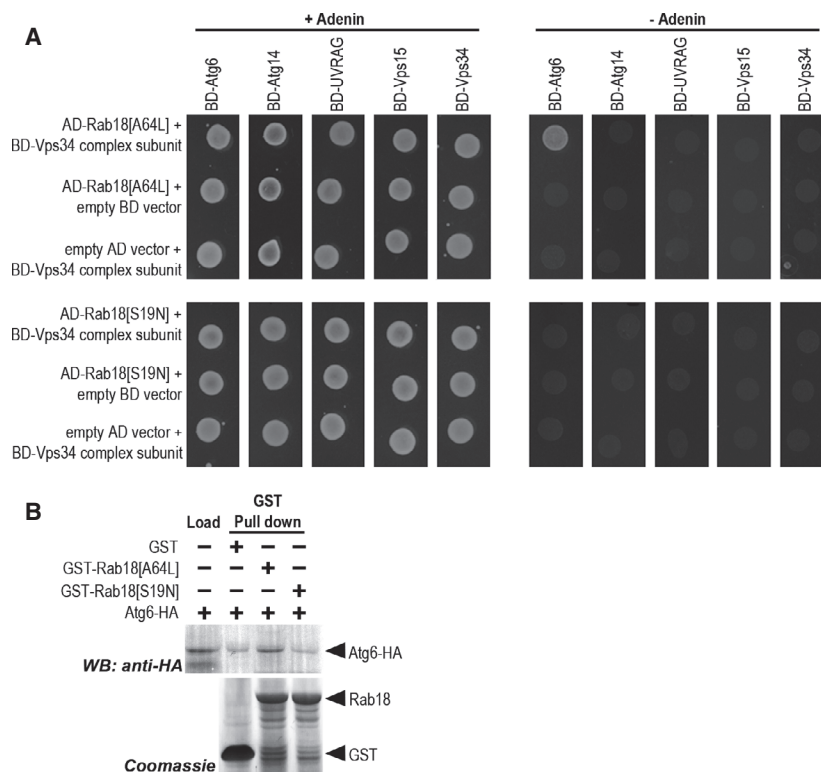


Fig. 9. Active Rab18 binds to the Vps34 complex subunit Atg6. (A) In yeast two-hybrid experiments, Rab18[A64L], the GTP-locked mutant form of Rab18, specifically bound the universal Vps34 complex subunit Atg6, while the GDP-locked Rab18[S19N] did not show any interaction. (B) Fly lysate-derived Atg6-HA preferentially binds to the GTP-locked mutant form of Rab18 in a GST pull-down assay. All experiments were done twice, and representative data are shown.

[5], our findings suggest that the Vps34 Complex I can be considered as a novel Rab18 effector.

Elevating endosomal membrane level of PI3P produced by the Rab5 effector Vps34 Complex II facilitates early-to-late endosome transition and promotes the Rab5-to-Rab7 switch [19,32]. This maturation step prepares the endosome for its subsequent fusion with lysosomes. Vps34 Complex I activity is considered as a source of autophagosomal PI3P required for autophagosome formation and maturation. Others and we found that matured autophagosomes also become positive for Rab7 [19,36], which may determine the fate of autophagosomes for fusion as well. If the Rab3GAP-Rab18 module – together with the Vps34 Complex I – plays a role in lysosome/autolysosome maturation, they should localize to the maturing autophagosomes or endosomes. To test this hypothesis, we immunolabeled Rab7 in fat tissues expressing Atg14, Rab3GAP2, or Rab18 reporters and observed that all reporters partially overlapped with Rab7 (Fig. 10A–C). Additionally, we also found partial colocalization between YFP-Rab18 and the Atg6-HA or Atg14-HA reporters (Fig. 10D,E), suggesting that these factors coexist on the same compartment.

Interestingly, the overlap between Rab3GAP-Rab18 module subunits and Rab7 was detectable in two distinct patterns. The first subset consisted of small

Rab3GAP2 and Rab18 patches on the surface of large Rab7-positive structures, likely representing matured lysosomes/autolysosomes. In contrast, the other subset appeared as small punctate structures on which the two markers fully overlapped (Fig. 10B,C). To elucidate whether these small Rab7 and Rab3GAP2 or Rab18 double-positive punctate structures represent small endosomes or autophagosomes, we performed immunolabeling experiments on Syx17 and It/Vps41 mutant backgrounds. Syx17 is a SNARE protein and It is a subunit of the HOPS tethering complex, both factors being essential mediators of autophagosome–lysosome fusion. In cells deficient for these genes, autophagosome–lysosome fusion is blocked [37–39], and as a result, large amounts of matured, Rab7-positive autophagosomes accumulate in a perinuclear pattern [19]. Interestingly, we found that Rab7 and the endogenous autophagosome marker Atg8a extensively colocalized with both the Rab3GAP2-GFP and the YFP-Rab18 reporters (Fig. 10F–I), highlighting that the Rab3GAP-Rab18 module is present on autophagosomes.

Discussion

In this study, we demonstrate that Rab3GAP2 mutant fruit flies display ataxia and may be used as an

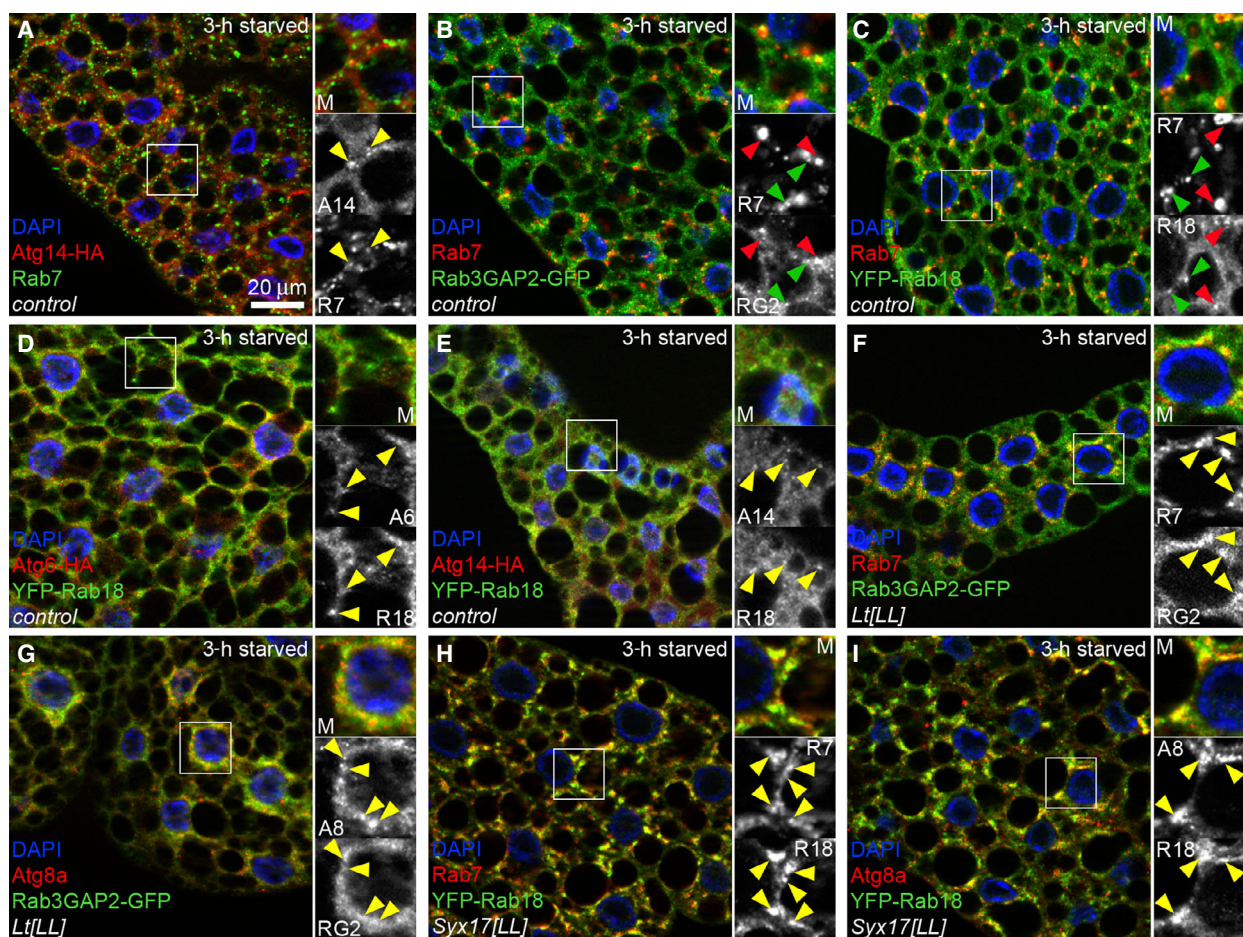


Fig. 10. Rab3GAP2-Rab18 module members and the Vps34 Complex I coexist on the same compartment and localize to Rab7-positive structures. (A) Atg14-HA colocalizes with a portion of Rab7-positive structures in the fat tissue of 3-h starved control larvae. (B, C) Rab3GAP2-GFP (B)- and YFP-Rab18 (C)-positive patches are visible on the surface of large Rab7-positive lysosomes (red arrowheads). Additionally, Rab3GAP2 and Rab18 reporters show full overlap with a cohort of small Rab7-positive structures (green arrowheads), which likely represent endosomes or autophagosomes. (D, E) Partial colocalization is detected between YFP-Rab18 and the Vps34 complex subunit reporters Atg6-HA (D) or Atg14-HA (E). (F, G) On an autophagosome–lysosome fusion defective *It* mutant genetic background, Rab3GAP2-GFP colocalization with Rab7 is retained (F) and also shows overlap with the endogenous autophagosomal marker Atg8a (G). (H) YFP-Rab18 colocalization with Rab7 is retained on a *Syx17* mutant genetic background in which autophagosome–lysosome fusion is blocked. (I) Rab18 also overlaps with the endogenous autophagosomal marker Atg8a in *Syx17* mutant fat tissue. Small panels in A–I show enlarged merged and grayscale views of red and green channels of the boxed areas. Arrowheads (in every color) indicate colocalizing objects in A–I. Scale bar in A is the same for B–I. All experiments were done twice, and representative data are shown.

invertebrate model system for WMS. Furthermore, the climbing defect may at least in part arise due to an autophagy failure obvious in adult muscle and larval fat cells. Our finding that the accumulation of p62 and Atg8a was not apparent in Rab3GAP2 mutant head lysates was surprising; but, it is possible that only a subset of neurons is defective for autophagy in these flies, which we failed to detect. Although studies in mammalian WMS models are focusing on neuronal defects [2,40], our data suggest that it may be worth to investigate other tissues of WMS patients as well.

For characterizing the role of the Rab3GAP-Rab18 module in autophagy, we used the genetically mosaic fat tissue of L3 larvae, a well-established system for autophagy analysis in *Drosophila*. By analyzing Rab3GAP2 mutants and multiple independent RNAi lines, we show that the loss-of-function cells are less effective in autophagosome–lysosome fusion and are defective in autolysosome morphology and maturation. Additionally, we found that the lack of Rab3GAP2 function causes striking perturbation of Rab7-positive late endosomes, autophagosomes, and (auto)lysosomes, but

it does not affect Rab5-positive early endosomes. Thus, our data suggest that the Rab3GAP-Rab18 module can be considered as a general regulator of lysosome maturation. These results fit well with the findings of a recently published paper showing that Rab18 acts in concert with Rab7 during the lysosomal fusion events of autophagy and in the axonal transport of lysosomes [41]. On the other hand, previous studies in *C. elegans* and cultured human cells suggested that the Rab3GAP subunits and Rab18 are rather involved in early steps of autophagy; however, it is important to note that these latter studies focused only on the amount and localization patterns of the autophagy markers Atg8 and p62, with no particular emphasis on ultrastructural analysis of the integrity of the lysosomal system [28,29]. Our electron microscopy observations concerning that numerous autophagosomes and autophagosome clusters are present in the cytoplasm of Rab3GAP2 mutant fat cells further suggest that loss of the Rab3GAP-Rab18 module causes major defects in (auto)lysosome function rather than in autophagosome formation. Of course, we cannot rule out the possibility that the discrepancies between these studies arise due to a tissue-specific role of the Rab3GAP-Rab18 module in autophagy. Our finding that Rab3GAP2 mutant adults obviously accumulate much more autophagy cargos in muscles than in their brain further corroborates this notion.

Since we demonstrated that loss of Vps34 Complex I function results in phenotypes similar to those of inhibition of the Rab3GAP-Rab18 module and, furthermore, a physical interaction between the permanent Vps34 complex subunit Atg6 and the GTP-bound Rab18 was proven, we propose that Complex I is likely a novel Rab18 effector.

Vps34 Complex I is one of the most important regulators of autophagosome formation, and it also has a role in autophagosome maturation and fusion [42]. As matured, intact autophagosomes in Rab3GAP2 mutant cells were detected, it seems likely that Rab18 is critical for Vps34 Complex I activity following autophagosome formation. Localization of Rab3GAP subunits and Rab18 to autophagosomes also suggests that this module plays a role in later steps of autophagosome maturation: It facilitates their fusion with lysosomes and further enhances the maturation of the newly formed autolysosomes into enlarged degradative compartments.

How could the autophagosome-localized Rab3GAP-Rab18 module affect vesicle maturation is yet to be answered. Based on our results showing that Rab7 becomes dispersed in cells lacking the Rab3GAP-Rab18 module, we suggest that the most important

role of this module is to stabilize the Rab7-containing compartment. During their maturation, (auto)lysosomes undergo a series of membrane fusion events with endosomes, Golgi-derived vesicles, and autophagosomes. All these steps are mediated by Rab7 and its effectors such as the tethering factor HOPS complex or the adaptor protein PLEKHM1 [38,43]. As matured autophagosomes are also positive for Rab7, the autophagy-derived Rab7 proteins can be an important source for the lysosomal Rab7 pool. This scenario is even more likely in cell types such as fat cells, which show relatively low endocytic but high autophagic activity. Still, we cannot rule out that the Rab3GAP-Rab18 complex is also present on maturing endosomes or Golgi-derived transport vesicles that may also act as important Rab7 sources for maturing lysosomes. The precise contribution of these membrane transport pathways to maintaining the lysosomal Rab7 pool needs to be further investigated in the future.

Our research highlights that the Rab3GAP-Rab18 module, in concert with the activity of the Vps34 Complex I, maintains the integrity of the Rab7-positive late endosomal/lysosomal compartment. Additionally, our findings that loss of Rab3GAP-Rab18 function perturbs autolysosome maturation and autophagic degradation shed light on a new possible cause of WMS development and open up potential novel therapeutic perspectives for this disease.

Materials and methods

Fly work

Flies were kept on standard cornmeal/yeast/agar medium at 22 °C. For starvation, adult flies were kept in empty vials for 3 h before the experiments. All larval experiments, if not otherwise stated, were performed on early L3-staged larvae following 3 h of starvation in 20% sucrose solution.

Mi[MIC]Rab3-GAP^{M111001} (called *Rab3GAP2[MI]* in text) and *Df(2L)ED761 (Rab3GAP2[Df])* mutants, *TRiP.JF01601 (UAS-Rab3GAP2 RNAi)* and *TRiP.JF02744 (UAS-Rab18 RNAi)* RNAi lines, *UASp-YFP-Rab3[Q80L]*, *UASp-YFP-Rab18[A64L]*, and *UAS-YFP-Rab18[S19N]* reporters, and *TI[TI]Rab18EYFP (YFP-Rab18)* YFP knock-in lines were obtained from Bloomington Drosophila Stock Center (Bloomington, IN, USA). *GD12118 (UAS-Rab3GAP2 RNAi/2)*, *GD10218 (UAS-Rab18 RNAi/2)*, *GD10413 (UAS-Rab3GAP1 RNAi/2)*, and *KK100903 (UAS-Atg14 RNAi)* RNAi lines and the *PBac[fTRG00724.sjGFP-TVPTBF]VK00033 (Rab3GAP2-GFP)* reporter line were ordered from Vienna Drosophila Resource Center (Vienna, Austria). *31935R-3 (UAS-Rab3GAP1 RNAi)* RNAi line was from National Institute of Genetics (NIG-Fly,

Table 1. List of the detailed genotypes used for the experiments

Figure	Panel	Genotype
1	A ('control')	w[1118]/w[1118]; +/-Rab3GAP2[Df]; +/-
	A ('Rab3GAP2[MII]/Df')	w[1118]/w[1118]; Rab3GAP2[MII]/Rab3GAP2[Df]; +/-
	C ('control')	w[1118]/w[1118]; +/-Rab3GAP2[Df]; +/-
	C ('Rab3GAP2[MII]/Df')	w[1118]/w[1118]; Rab3GAP2[MII]/Rab3GAP2[Df]; +/-
	D	w[1118]/w[1118]; +/-Rab3GAP2[Df]; +/-
2	E	w[1118]/w[1118]; Rab3GAP2[MII]/Rab3GAP2[Df]; +/-
	A	w[1118]/w[1118]; +/-; 3xmCherry-Atg8a/3xmCherry-Atg8a
	B	w[1118]/w[1118]; Rab3GAP2[MII]/Rab3GAP2[MII]; 3xmCherry-Atg8a/3xmCherry-Atg8a
	D	w[1118], hs-Flp/w[1118]; UAS-2xEGFP, 3xmCherry-Atg8a/+; Act>CD2>Gal4, UAS-Dcr2/UAS-Rab3GAP2 RNAi
	E	w[1118], hs-Flp/w[1118]; UAS-2xEGFP, 3xmCherry-Atg8a/UAS-Rab3GAP2 RNAi/2; Act>CD2>Gal4, UAS-Dcr2/+
	F	w[1118], hs-Flp/w[1118]; UAS-2xEGFP, 3xmCherry-Atg8a/+; Act>CD2>Gal4, UAS-Dcr2/UAS-Rab3GAP1 RNAi
	G	w[1118], hs-Flp/w[1118]; UAS-2xEGFP, 3xmCherry-Atg8a/+; Act>CD2>Gal4, UAS-Dcr2/UAS-Rab3GAP1 RNAi/2
	H	w[1118], hs-Flp/w[1118]; UAS-2xEGFP, 3xmCherry-Atg8a/+; Act>CD2>Gal4, UAS-Dcr2/UAS-Rab18 RNAi
	I	w[1118], hs-Flp/w[1118]; UAS-2xEGFP, 3xmCherry-Atg8a/+; Act>CD2>Gal4, UAS-Dcr2/UAS-Rab18 RNAi/2
	K ('control')	w[1118]/w[1118]; +/-Rab3GAP2[MII]; +/-
	K ('Rab3GAP2[MII]/Df')	w[1118]/w[1118]; Rab3GAP2[MII]/Rab3GAP2[Df]; +/-
K ('Rab3GAP2[MII]/Df rescue')	w[1118]/w[1118]; Rab3GAP2[MII]/Rab3GAP2[Df]; Rab3GAP2-GFP/+	
3	A	w[1118], hs-Flp/w[1118]; FRT40A tub-QS/FRT40A Rab3GAP2[MII]; ET49-QF, QUAS-GFP/+
	B	w[1118], hs-Flp/w[1118]; UAS-2xEGFP/+; Act>CD2>Gal4, UAS-Dcr2/UAS-Rab3GAP2 RNAi
	C	w[1118], hs-Flp/w[1118]; UAS-2xEGFP/+; Act>CD2>Gal4, UAS-Dcr2/UAS-Rab3GAP1 RNAi
	D	w[1118], hs-Flp/w[1118]; UAS-2xEGFP/+; Act>CD2>Gal4, UAS-Dcr2/UAS-Rab18 RNAi
	E	w[1118]/w[1118]; +/-; Lamp-3xmCherry/Lamp-3xmCherry
	F	w[1118]/w[1118]; Rab3GAP2[MII]/Rab3GAP2[MII]; Lamp-3xmCherry/Lamp-3xmCherry
	G	w[1118], hs-Flp/w[1118]; UAS-2xEGFP, Lamp-3xmCherry/+; Act>CD2>Gal4, UAS-Dcr2/UAS-Rab3GAP2 RNAi
	H	w[1118], hs-Flp/w[1118]; UAS-2xEGFP, Lamp-3xmCherry/+; Act>CD2>Gal4, UAS-Dcr2/UAS-Rab3GAP1 RNAi
	I	w[1118], hs-Flp/w[1118]; UAS-2xEGFP, Lamp-3xmCherry/+; Act>CD2>Gal4, UAS-Dcr2/UAS-Rab18 RNAi
4	A	w[1118]/w[1118]; +/-; 3xmCherry-Atg8a/3xmCherry-Atg8a
	B	w[1118]/w[1118]; Rab3GAP2[MII]/Rab3GAP2[MII]; 3xmCherry-Atg8a/3xmCherry-Atg8a
	C	w[1118], hs-Flp/w[1118]; UAS-GFP-Lamp1, 3xmCherry-Atg8a/+; Act>CD2>Gal4, UAS-Dcr2/+
	D	w[1118], hs-Flp/w[1118]; UAS-GFP-Lamp1, 3xmCherry-Atg8a/+; Act>CD2>Gal4, UAS-Dcr2/UAS-Rab3GAP2 RNAi
	E	w[1118], hs-Flp/w[1118]; UAS-GFP-Lamp1, 3xmCherry-Atg8a/+; Act>CD2>Gal4, UAS-Dcr2/UAS-Rab3GAP1 RNAi
	I	w[1118], hs-Flp/w[1118]; UAS-GFP-Lamp1, 3xmCherry-Atg8a/+; Act>CD2>Gal4, UAS-Dcr2/UAS-Rab18 RNAi
5	A	w[1118]/w[1118]; +/-Rab3GAP2[MII]; +/-
	B	w[1118]/w[1118]; Rab3GAP2[MII]/Rab3GAP2[Df]; +/-
	C	w[1118], hs-Flp/w[1118]; UAS-2xEGFP, Lamp-3xmCherry/+; Act>CD2>Gal4, UAS-Dcr2/UAS-Rab3GAP1 RNAi
6	A	w[1118], hs-Flp/w[1118]; FRT40A tub-QS/FRT40A Rab3GAP2[MII]; ET49-QF, QUAS-GFP/+
	C	w[1118], hs-Flp/w[1118]; FRT40A tub-QS/FRT40A Rab3GAP2[MII]; ET49-QF, QUAS-GFP/+
	E	w[1118], hs-Flp/w[1118]; FRT40A tub-QS/FRT40A Rab3GAP2[MII]; ET49-QF, QUAS-GFP/+
	G	w[1118]/w[1118]; +/-Rab3GAP2[MII]; +/-
	H	w[1118]/w[1118]; Rab3GAP2[MII]/Rab3GAP2[MII]; +/-

Table 1. (Continued).

Figure	Panel	Genotype
7	A	w[1118], hs-Flp/w[1118]; UAS-2xEGFP, Lamp-3xmCherry/UAS-Atg14 RNAi; Act>CD2>Gal4, UAS-Dcr2/+
	B	w[1118], hs-Flp/w[1118]; UAS-2xEGFP, Lamp-3xmCherry/+; Act>CD2>Gal4, UAS-Dcr2/UAS-FLAG-UVRAG
	C	w[1118], hs-Flp/w[1118]; UAS-2xEGFP/UAS-Atg14 RNAi; Act>CD2>Gal4, UAS-Dcr2/+
	D	w[1118], hs-Flp/w[1118]; UAS-2xEGFP/+; Act>CD2>Gal4, UAS-Dcr2/UAS-FLAG-UVRAG
	E	w[1118]/w[1118]; +/-; +/-
	F	w[1118]/w[1118]; +/-; Atg14[d13]/Atg14[d13]
8	A	w[1118], hs-Flp/w[1118]; UAS-2xEGFP/UAS-Atg14 RNAi; Act>CD2>Gal4, UAS-Dcr2/+
	B	w[1118], hs-Flp/w[1118]; UAS-2xEGFP/+; Act>CD2>Gal4, UAS-Dcr2/UAS-FLAG-UVRAG
	C	w[1118], hs-Flp/w[1118]; UAS-2xEGFP, 3xmCherry-Atg8a/+; Act>CD2>Gal4, UAS-Dcr2/UAS-FLAG-UVRAG
	F	w[1118], hs-Flp/w[1118]; UAS-2xEGFP, Lamp-3xmCherry/+; Act>CD2>Gal4, UAS-Dcr2/UAS-FLAG-UVRAG
9	B	w[1118]/w[1118]; +/-; Atg6-HA/Atg6-HA
10	A	w[1118]/w[1118]; Atg14-HA/Atg14-HA; Atg14-HA/Atg14-HA
	B	w[1118]/w[1118]; +/-; Rab3GAP2-GFP/Rab3GAP2-GFP
	C	YFP-Rab18, w[1118]/YFP-Rab18, w[1118]; +/-; +/-
	D	YFP-Rab18, w[1118]/YFP-Rab18, w[1118]; +/-; Atg6-HA/Atg6-HA
	E	YFP-Rab18, w[1118]/YFP-Rab18, w[1118]; Atg14-HA/Atg14-HA; Atg14-HA/Atg14-HA
	F	w[1118]/w[1118]; Lt[LL]/Lt[LL]; Rab3GAP2-GFP/Rab3GAP2-GFP
	G	w[1118]/w[1118]; Lt[LL]/Lt[LL]; Rab3GAP2-GFP/Rab3GAP2-GFP
	H	YFP-Rab18, w[1118]/YFP-Rab18, w[1118]; +/-; Syx17[LL]/Syx17[LL]
	I	YFP-Rab18, w[1118]/YFP-Rab18, w[1118]; +/-; Syx17[LL]/Syx17[LL]

Mishima, Japan). The *UAS* enhancer-driven FLAG-tagged *UVRAG* reporter line [44] was a gift from S. Choi. The *UAS-GFP-Lamp1* reporter line [45] was kindly provided by Helmut Kramer. Endogenous promoter-driven *3xmCherry-Atg8a* and *Lamp-3xmCherry* reporters and the *Atg14[d13]*, *Syx17[LL06330]*, and *Lt[LL07138]* (called as *Syx17[LL]* and *Lt[LL]* in the text) mutant lines were described earlier [19,37,46]. Endogenous promoter-driven C-terminally 3xHA-tagged *Atg14* and *Atg6* reporter lines were generated for our earlier [19] and present studies, respectively.

Mosaic larvae carrying randomly generated Gal4-expressing fat cell clones were made by the utilization of *Hsp70-Flp*, *Act-FRT-CD2-FRT-Gal4* technique [30]. *Rab3GAP2* homozygous mutant fat cell clones were generated by MARCM strategy: *FRT40A Rab3GAP2[MI]* flies were crossed with a *Hsp70-Flp*; *FRT40A tub-QS*; *ET49-QF*, *QUAS-GFP* line [19] and F1 generation was heat-shocked at embryonic stage (4 h after egg laying) for 45 min in 37 °C water bath. All genotypes used in this study are listed in detail in Table 1.

For climbing tests, 8- and 32-day-old male flies climbed vertically in a plastic tube. Thirty flies climbed in cohorts (6 flies/cohort) per genotype, each fly climbed three times. All climbings were recorded as 10- to 15-second-long video clips. At the zero time point, flies were shaken off to the bottom of the tube and climbing speed was calculated based on the cumulative vertical climbing distance made by each individual flies in the first 5 s.

Histology and imaging

For LTR stainings, starved L3 larvae were dissected and their isolated fat bodies were incubated in LTR (1 : 5000; Thermo Fisher, Waltham, Ma, USA)-PBS staining solution for 5 min, rinsed once in PBS, and mounted in mounting media (1 : 1 glycerol-PBS) containing 0.2 µg·mL⁻¹ DAPI.

For immunostaining of thoracic muscles, the head, abdomen, and legs were removed from 30-day-old adult male flies. Then, the thoraxes were placed into a drop of PBS and bisected in the midline by a sharp blade. The half thoraxes were fixed in 4% formaldehyde-PBS for 30 min at room temperature. For immunostainings of larval fat bodies, starved L3 larvae were inverted and fixed in 4% formaldehyde-PBS for 45 min at room temperature. The remaining steps of the staining method were the same for both tissue types, and it was described earlier [20]. The following primary antibodies were used: chicken polyclonal anti-GFP (1 : 1000; Thermo Fisher), rat polyclonal anti-Atg8a (1 : 300) [37], rabbit polyclonal anti-p62 (1 : 1000) [47], rabbit polyclonal anti-Rab5 (1 : 100; ab31261; Abcam, Cambridge, UK), mouse monoclonal anti-Rab7 (1 : 10; DSHB, Iowa City, IA, USA), rabbit polyclonal anti-Arl8 (1 : 300; DSHB), rabbit polyclonal anti-Cathepsin L (1 : 100; ab58991, Abcam), and rabbit polyclonal anti-HA (1 : 100; Merck, Darmstadt, Germany). The following secondary antibodies were used: Alexa Fluor 488 goat anti-chicken; Alexa Fluor 488 goat anti-mouse; Alexa Fluor 488

goat anti-rat; Alexa Fluor 488 goat anti-rabbit; Alexa Fluor 568 goat anti-rabbit; and Alexa Fluor 568 goat anti-mouse (1 : 1000 for all; all from Thermo Fisher).

Images were taken by Axio Imager M2 Fluorescent microscope, running ZEN 2.3 software and equipped with Plan-Apochromat 40×/0.95 Air Objective, Apotome 2 confocal unit (all from Zeiss, Jena, Germany), and Orca Flash 4.0 LT sCMOS camera (Hamamatsu Photonics, Hamamatsu City, Japan). High-magnification Z-stack images used for 3D rendering were taken by Zeiss LSM 800 equipped with a Plan-Apochromat 63×/1.4 objective. Images were processed by ZEN LITE (Zeiss) and PHOTOSHOP (Adobe, San Jose, CA, USA) softwares.

Electron microscopy

For ultrastructural analysis, the preparation of larval fat body samples was carried out as it was described earlier [20]. Briefly, fat bodies were dissected and fixed in 3.2% PFA, 1% glutaraldehyde, 1% sucrose, and 0.028% CaCl₂ in 0.1 N sodium cacodylate, pH 7.4, overnight at 4 °C. Then, the samples were undergone postfixation in 0.5% osmium tetroxide for 1 h and in half-saturated aqueous uranyl acetate for 30 min at room temperature. The samples were dehydrated in a graded series of ethanol and embedded in Durcupan resin (Merck) by following the manufacturer's recommendations. Ultrasections were stained with Reynolds' lead citrate. Sample preparation and performing correlative EM were done as it was described earlier [19,48]. Samples were analyzed with JEM-1011 transmission electron microscope (Jeol, Akishima, Japan), and images were acquired with a Morada digital camera (Olympus, Shinjuku City, Japan) running ITEM software (Olympus).

Molecular cloning

For generating endogenous promoter-driven, C-terminally 3xHA-tagged Atg6 transgene, the genomic locus of Atg6 gene (covering the region between the 1131th nucleotide upstream of the transcription start site and the last amino acid coding codon; primers: 5'-GCGGCCGCATGGC GCGCCCGGTGACACAACTGTGAAGAAACC-3' and 5'-GCGGCCGCGCGCGCCTCTGGCGCGATAAATT CGGCT-3') was PCR-amplified and cloned into the AscI site of the previously described gen3xHA vector [19].

For yeast two-hybrid experiments, Vps34 complex subunits were PCR-amplified from cDNA derived from the GH13170, LD35669, LD05963, and LD37690 EST clones (Drosophila Genomics Resource Center, Bloomington, IN, USA) for Vps34, Atg6, UVRAG, and Atg14, respectively. Vps15 A isoform cDNA was a gift of T. E. Rusten. Amplified sequences were cloned into the pGBKT7 BD (Gal4 DNA-binding domain) vector (Clontech, Mountain View, CA, USA) using the following restriction sites: NdeI-EcoRI

for Vps34 (primers: 5'-CTGCTTCATATGGACCAGCCC-GACGACCATTTCCTCG-3' and 5'-ACTGTACATATGGA ATTCTACTTCCGCCAGTATTGGGTGAACC-3'), NdeI-SalI for Atg6 (primers: 5'-ACTGATGAATTCCA TATGAGTGAGGCGGAAAAGCAGGCGGTGTC-3' and 5'-CTGACTGGATCCGTCGACCTCACGGTGACACAA ACTGTGAAGAAACC-3') and for Vps15 A isoform (primers: 5'-CTGATTCATATGGGCAATCAACTGGTGGGC -3' and 5'-ACTGATCATATGTCGACATCACTTCCAC AGCTTGATGACACCGT-3'), NdeI-XhoI for UVRAG (primers: 5'-ACAGTATCATATGAATCTACGGCCGCG ATGCC-3' and 5'-AGATGACTCGAGTCAGTCGCGCT CAGTTTGCAGA-3'), and EcoRI-SalI for Atg14 (primers: 5'-CCATGGAATTCATATGGCAAACAGCTCCAGCT CCG-3' and 5'-ATCAGTCGACTCATTGATCCAGCG CAGCAC-3').

Point mutant Rab18 forms were PCR-amplified using genomic DNA as template isolated from the UAS-YFP-Rab18[A64L] GTP-locked and the UAS-Rab18[S19N] GDP-locked Rab18 mutant transgene-carrying fly stocks (primers: 5'-ACTGAGAATTCATGGCTGATCGGGCTA TCAAGCTG-3' and 5'-CTGACTGGATCCCTCGAGGT CAACAGTAACACGTAGACGCGCTTGCC-3'), and cloned into the EcoRI-XhoI sites of the pGADT7 AD (Gal4 activation domain) vector (Clontech). All transgenes were verified by sequencing and we noticed that both AD-Rab18 transgenes carried a T>C base substitution at the 23th position downstream of the translation start, causing an amino acid change from leucine to proline in the 8th position (L8P). This mutation was restored in both clones by QuikChange™ (Agilent, Santa Clara, CA, USA) site-directed mutagenesis (primers: 5'-GATCGGGCTATCAA GCTGCTGGTATCGGGGAA-3' and 5'-TTCCCGCAT CACCAGCAGCTTGATAGCCCGATC-3') according to the corresponding wild-type *Drosophila* Rab18 sequence annotated in FlyBase. GST-tagged Rab18 GTP- and GDP-locked mutant transgenes were generated by PCR amplification of full-length Rab18 forms using the above-described QuikChange-corrected Rab18[A64L] and Rab18[S19N] transgenes as templates (primers: 5'-CAGGGATCCAT GGCTGATCGGGCT-3' and 5'-GTGCTCGAGACAG TAACACGTAGA-3'). The PCR products were inserted between the BamHI and XhoI restriction sites of the pETARA expression vector-containing DNA sequences for N-terminal Glutathione S-transferase and a C-terminal hexahistidine tag [49].

Biochemistry

Rosetta™ (DE3) competent *Escherichia coli* cells (Merck) were used for expression of Rab18[A64L] and Rab18 [S19N] proteins tagged with N-terminal GST and C-terminal hexahistidine. Cells were grown on 37 °C until OD₆₀₀ reached 0.4–0.6. Protein expression was induced overnight at 18 °C with 0.05 mM IPTG. After expression, the cells

were harvested by centrifugation at 3315 *g* for 5 min with Beckman JLA 9.1000 rotor (Beckman Coulter Life Sciences, Indianapolis, IN, USA), resuspended in PBS, and centrifuged again at 1878 *g* for 5 min with Eppendorf F-35-6-30 rotor (Eppendorf, Hamburg, Germany). The supernatant was decanted, and the pelleted cells were stored at -80°C until further use.

For pull-down experiments, pelleted Rab18[A64L]- and Rab18[S19N]-expressing cells were resuspended in lysis buffer (50 mM Na_2HPO_4 pH = 8, 300 mM NaCl, 20 mM imidazole, 0.1% Triton X-100, 2 mM β -mercaptoethanol) containing 200 μM GTP or GDP, respectively. Cells were lysed by freeze–thaw cycles followed by sonication, and then, the samples were centrifuged at 30 130 *g* for 30 min with Eppendorf FA-45-24-11-HS rotor at 4°C . The supernatant was collected and mixed with Glutathione Sepharose™ High-Performance resin (GE Healthcare, Chicago, IL, USA) and then incubated at 4°C for 1 h with rotation. Once incubation was finished, whole-body lysates (see below) of adult flies expressing *Atg6-3xHA* reporter from endogenous promoter-driven transgene were mixed with Glutathione Sepharose resin saturated with the given mutant Rab18 protein and then incubated for 30 min with rotation. The samples were applied for gravity flow column followed by successive washes with lysis buffer elution with Laemmli buffer and finally were applied for western blot analysis.

For preparing lysates, 2-day-old adult flies carrying the *Atg6-HA* transgene were collected to plastic tubes, weighed, and 1.2 mL ice-cold lysis buffer was added to 120 mg of flies. They were homogenized with Ultra-Turrax T10 using an S10N-5G disperser (both from IKA, Staufen, Germany) and centrifuged at 30 130 *g* for 10 min at 4°C . About 650 μL of clean supernatant was collected from each 1.2 mL of samples.

For preparing western blot samples, early L3 larvae were firstly washed in PBS and dried on filter paper, and then flies or larvae were collected into plastic tubes and weighed. After addition of 2xLaemmli-PBS (1 : 1) solution (20 μL per sample mg), samples were boiled for 5 min at 100°C and homogenized. Then, the samples were boiled again and centrifuged at 16 627 *g* for 5 min with Eppendorf FA-45-24-11-HS rotor. Finally, supernatants were collected to a new plastic tube and stored at -20°C . During the preparation of adult head and body samples, heads were displaced from bodies and collected into separate plastic tubes on ice. The bodies were weighted, and 20 μL per sample mg of 2xLaemmli-PBS (1 : 1) solution was added. For head samples, 2.5 μL /head of 2xLaemmli-PBS (1 : 1) was added, and then both head and body samples were treated the same way as whole-larval samples.

Western blotting was performed using Mini-PROTEAN Tetra Cell and Trans-Blot Turbo Transfer systems (both from Bio-Rad, Hercules, CA, USA) by following the manufacturer's instructions and standard protocols. The

following primary antibodies were used: rabbit polyclonal anti-p62 (1 : 3000) [47]; mouse monoclonal anti-tubulin (1 : 2000; AA4.3-s, DSHB); rat monoclonal anti-HA (1 : 2000; 3F10, Roche, Basel, Switzerland); and rabbit monoclonal anti-Gabarap+GabapL1+GabapL2 (1 : 5000; ab109364, Abcam) was used for Atg8a detection. The following secondary antibodies were used: alkaline phosphatase-conjugated anti-rabbit, anti-rat, and anti-mouse (all 1 : 5000; Merck). The blots were developed by alkaline phosphatase reaction with NBT/BCIP chromogenic substrate.

Yeast two-hybrid experiments

The Vps34 complex subunits (cloned into pGBKT7 BD vectors) and the GTP- and GDP-locked mutant forms of Rab18 (cloned into pGADT7 AD vectors) were transformed into the yeast strain AH109 using the Frozen-EZ Yeast Transformation II Kit (Zymo Research, Irvine, CA, USA). The transformants were selected by growth on minimal medium lacking Trp and Leu (SD-WL). To detect protein–protein interaction on the basis of reporter gene expression, transformants were grown on selective minimal medium lacking Trp, Leu, and Ade (SD-WLA). Empty vectors were used as negative controls.

Statistics

We quantified the number and size of fluorescent structures from original, unmodified pictures by using IMAGEJ (National Institutes of Health, Bethesda, MD, USA). The threshold was set manually by the same person working in a dark room. We considered a structure as lysosomal/autolysosomal chain if it consisted of 3 or more spherical shaped substructures where the distance between the spheres was smaller than the diameter of the individual puncta. For quantification of the number of lysosomal/autophagic connections represented in diagrams, we counted manually the number of the connections and connecting points between these spherical substructures and the single tubules emanating from solitary lysosomes/autolysosomes. Numbers of Rab5 or Rab7 puncta were counted in IMAGEJ. In case of clonal experiments, randomly chosen RNAi-silenced, mutant or transgene-overexpressing cells and their neighboring control cells were quantified. The data pairs were corrected by cell size ratio. In case of area-based quantification, we randomly chose 300×300 pixel areas for calculating number and size of fluorescent structures. For quantification of colocalization, 120–150 puncta were randomly chosen and counted on 10 images per genotype.

Data were imported to SPSS STATISTICS (IBM, Armonk, NY, USA) and were tested for normality of data distribution. Then, we calculated *P*-values with the appropriate statistical tests: Two-tailed, two-sample, unequal variance *t*-test was used for comparison of two Gaussian datasets, or

Mann–Whitney (*U*) test was used when at least one of the two datasets showed non-normal distribution. *P*-values are represented over the clasps linking data pairs in every diagram.

Acknowledgements

We thank Sarolta Palfia for the excellent technical assistance and colleagues and stock centers listed in the [Materials and methods](#) section for providing reagents. This work was supported by the Hungarian Academy of Sciences [LP-2014/2 to GJ, PPD-003/2016 to ST, PPD-222/2018 to PL, BO/00652/17 to ZSV.]; the National Research, Development and Innovation Office of Hungary [GINOP-2.3.2-15-2016-00006 and -00032, K119842, and KKP129797 to GJ, KH125108 to ST, PD124594 to ZSV]; and the ÚNKP New National Excellence Program of the Ministry of Human Capacities of Hungary (ÚNKP-17-3-I-ELTE-27 and ÚNKP-18-3-I-ELTE-314 to AB, ÚNKP-18-4-ELTE-409 to ZSV.). The funders had no role in study design, data collection and analysis, decision to publish, or preparation of the manuscript.

Conflict of interest

The authors declare no conflict of interest.

Author contributions

STakats, LL, AB, SToth, ZS-V, AR, and PL performed the experiments. STakats, GG, and GJ planned the experiments. Data were quantified by LL, AB, and SToth. ZS-V, AV, ML, and GG produced the novel reagents described in this study. STakats and GJ wrote the manuscript. ML and AB contributed by essential revision of the manuscript. The research was conceived and designed by STakats and GJ.

References

- 1 Handley MT & Aligianis IA (2012) RAB3GAP1, RAB3GAP2 and RAB18: disease genes in Micro and Martsolf syndromes. *Biochem Soc Trans* **40**, 1394–1397.
- 2 Carpanini SM, McKie L, Thomson D, Wright AK, Gordon SL, Roche SL, Handley MT, Morrison H, Brownstein D, Wishart TM *et al.* (2014) A novel mouse model of Warburg Micro syndrome reveals roles for RAB18 in eye development and organisation of the neuronal cytoskeleton. *Dis Model Mech* **7**, 711–722.
- 3 Handley MT, Morris-Rosendahl DJ, Brown S, Macdonald F, Hardy C, Bem D, Carpanini SM, Borck G, Martorell L, Izzi C *et al.* (2013) Mutation spectrum in RAB3GAP1, RAB3GAP2, and RAB18 and genotype-phenotype correlations in warburg micro syndrome and Martsolf syndrome. *Hum Mutat* **34**, 686–696.
- 4 Liegel RP, Handley MT, Ronchetti A, Brown S, Langemeyer L, Linford A, Chang B, Morris-Rosendahl DJ, Carpanini S, Posmyk R *et al.* (2013) Loss-of-function mutations in TBC1D20 cause cataracts and male infertility in blind sterile mice and Warburg micro syndrome in humans. *Am J Hum Genet* **93**, 1001–1014.
- 5 Stenmark H (2009) Rab GTPases as coordinators of vesicle traffic. *Nat Rev Mol Cell Biol* **10**, 513–525.
- 6 Gerondopoulos A, Bastos RN, Yoshimura S, Anderson R, Carpanini S, Aligianis I, Handley MT & Barr FA (2014) Rab18 and a Rab18 GEF complex are required for normal ER structure. *J Cell Biol* **205**, 707–720.
- 7 Ozeki S, Cheng J, Tauchi-Sato K, Hatano N, Taniguchi H & Fujimoto T (2005) Rab18 localizes to lipid droplets and induces their close apposition to the endoplasmic reticulum-derived membrane. *J Cell Sci* **118**, 2601–2611.
- 8 Martin S, Driessen K, Nixon SJ, Zerial M & Parton RG (2005) Regulated localization of Rab18 to lipid droplets: effects of lipolytic stimulation and inhibition of lipid droplet catabolism. *J Biol Chem* **280**, 42325–42335.
- 9 Dejgaard SY, Murshid A, Erman A, Kizilay O, Verbich D, Lodge R, Dejgaard K, Ly-Hartig TB, Peppercok R, Simpson JC *et al.* (2008) Rab18 and Rab43 have key roles in ER-Golgi trafficking. *J Cell Sci* **121**, 2768–2781.
- 10 Hashim S, Mukherjee K, Rajee M, Basu SK & Mukhopadhyay A (2000) Live *Salmonella* modulate expression of Rab proteins to persist in a specialized compartment and escape transport to lysosomes. *J Biol Chem* **275**, 16281–16288.
- 11 Xu D, Li Y, Wu L, Li Y, Zhao D, Yu J, Huang T, Ferguson C, Parton RG, Yang H *et al.* (2018) Rab18 promotes lipid droplet (LD) growth by tethering the ER to LDs through SNARE and NRZ interactions. *J Cell Biol* **217**, 975–995.
- 12 Salloum S, Wang H, Ferguson C, Parton RG & Tai AW (2013) Rab18 binds to hepatitis C virus NS5A and promotes interaction between sites of viral replication and lipid droplets. *PLoS Pathog* **9**, e1003513.
- 13 Tang WC, Lin RJ, Liao CL & Lin YL (2014) Rab18 facilitates dengue virus infection by targeting fatty acid synthase to sites of viral replication. *J Virol* **88**, 6793–6804.
- 14 Klionsky DJ, Abdelmohsen K, Abe A, Abedin MJ, Abeliovich H, Acevedo, Arozana A, Adachi H, Adams CM, Adams PD, Adeli K *et al.* (2016) Guidelines for the use and interpretation of assays for monitoring autophagy. *Autophagy* **12**, 1–222.
- 15 Mizushima N, Levine B, Cuervo AM & Klionsky DJ (2008) Autophagy fights disease through cellular self-digestion. *Nature* **451**, 1069–1075.

- 16 Juhasz G, Erdi B, Sass M & Neufeld TP (2007) Atg7-dependent autophagy promotes neuronal health, stress tolerance, and longevity but is dispensable for metamorphosis in *Drosophila*. *Genes Dev* **21**, 3061–3066.
- 17 Kim M, Sandford E, Gatica D, Qiu Y, Liu X, Zheng Y, Schulman BA, Xu J, Semple I, Ro SH *et al.* (2016) Mutation in ATG5 reduces autophagy and leads to ataxia with developmental delay. *eLife* **5**, e12245.
- 18 Hara T, Nakamura K, Matsui M, Yamamoto A, Nakahara Y, Suzuki-Migishima R, Yokoyama M, Mishima K, Saito I, Okano H *et al.* (2006) Suppression of basal autophagy in neural cells causes neurodegenerative disease in mice. *Nature* **441**, 885–889.
- 19 Hegedus K, Takats S, Boda A, Jipa A, Nagy P, Varga K, Kovacs AL & Juhasz G (2016) The Ccz1-Mon1-Rab7 module and Rab5 control distinct steps of autophagy. *Mol Biol Cell* **27**, 3132–3142.
- 20 Lorincz P, Toth S, Benko P, Lakatos Z, Boda A, Glatz G, Zobel M, Bisi S, Hegedus K, Takats S *et al.* (2017) Rab2 promotes autophagic and endocytic lysosomal degradation. *J Cell Biol* **216**, 1937–1947.
- 21 Fujita N, Huang W, Lin TH, Groulx JF, Jean S, Nguyen J, Kuchitsu Y, Koyama-Honda I, Mizushima N, Fukuda M *et al.* (2017) Genetic screen in *Drosophila* muscle identifies autophagy-mediated T-tubule remodeling and a Rab2 role in autophagy. *eLife* **6**, e23367.
- 22 Jager S, Bucci C, Tanida I, Ueno T, Kominami E, Saftig P & Eskelinen EL (2004) Role for Rab7 in maturation of late autophagic vacuoles. *J Cell Sci* **117**, 4837–4848.
- 23 Lund VK, Madsen KL & Kjaerulf O (2018) *Drosophila* Rab2 controls endosome-lysosome fusion and LAMP delivery to late endosomes. *Autophagy* **14**, 1520–1542.
- 24 Itakura E, Kishi C, Inoue K & Mizushima N (2008) Beclin 1 forms two distinct phosphatidylinositol 3-kinase complexes with mammalian Atg14 and UVRAG. *Mol Biol Cell* **19**, 5360–5372.
- 25 Ohashi Y, Soler N, Garcia Ortegon M, Zhang L, Kirsten ML, Perisic O, Masson GR, Burke JE, Jakobi AJ, Apostolakis AA *et al.* (2016) Characterization of Atg38 and NRBF2, a fifth subunit of the autophagic Vps34/PIK3C3 complex. *Autophagy* **12**, 2129–2144.
- 26 Ohashi Y, Tremel S & Williams RL (2019) VPS34 complexes from a structural perspective. *J Lipid Res* **60**, 229–241.
- 27 Lorincz P, Lakatos Z, Maruzs T, Szatmari Z, Kis V & Sass M (2014) Atg6/UVRAG/Vps34-containing lipid kinase complex is required for receptor downregulation through endolysosomal degradation and epithelial polarity during *Drosophila* wing development. *Biomed Res Int* **2014**, 851349.
- 28 Feldmann A, Bekbulat F, Huesmann H, Ulbrich S, Tatzelt J, Behl C & Kern A (2017) The RAB GTPase RAB18 modulates macroautophagy and proteostasis. *Biochem Biophys Res Commun* **486**, 738–743.
- 29 Spang N, Feldmann A, Huesmann H, Bekbulat F, Schmitt V, Hiebel C, Koziollek-Drechsler I, Clement AM, Moosmann B, Jung J *et al.* (2014) RAB3GAP1 and RAB3GAP2 modulate basal and rapamycin-induced autophagy. *Autophagy* **10**, 2297–2309.
- 30 Juhasz G, Hill JH, Yan Y, Sass M, Baehrecke EH, Backer JM & Neufeld TP (2008) The class III PI(3)K Vps34 promotes autophagy and endocytosis but not TOR signaling in *Drosophila*. *J Cell Biol* **181**, 655–666.
- 31 Hyttinen JM, Niittykoski M, Salminen A & Kaarniranta K (2013) Maturation of autophagosomes and endosomes: a key role for Rab7. *Biochim Biophys Acta* **1833**, 503–510.
- 32 Poteryaev D, Datta S, Ackema K, Zerial M & Spang A (2010) Identification of the switch in early-to-late endosome transition. *Cell* **141**, 497–508.
- 33 Gillingham AK, Sinka R, Torres IL, Lilley KS & Munro S (2014) Toward a comprehensive map of the effectors of rab GTPases. *Dev Cell* **31**, 358–373.
- 34 Boda A, Lorincz P, Takats S, Csizmadia T, Toth S, Kovacs AL & Juhasz G (2019) *Drosophila* Arl8 is a general positive regulator of lysosomal fusion events. *Biochim Biophys Acta Mol Cell Res* **1866**, 533–544.
- 35 Li X, He L, Che KH, Funderburk SF, Pan L, Pan N, Zhang M, Yue Z & Zhao Y (2012) Imperfect interface of Beclin1 coiled-coil domain regulates homodimer and heterodimer formation with Atg14L and UVRAG. *Nat Commun* **3**, 662.
- 36 Pankiv S, Alemu EA, Brech A, Bruun JA, Lamark T, Overvatn A, Bjorkoy G & Johansen T (2010) FYCO1 is a Rab7 effector that binds to LC3 and PI3P to mediate microtubule plus end-directed vesicle transport. *J Cell Biol* **188**, 253–269.
- 37 Takats S, Nagy P, Varga A, Pircs K, Karpati M, Varga K, Kovacs AL, Hegedus K & Juhasz G (2013) Autophagosomal Syntaxin17-dependent lysosomal degradation maintains neuronal function in *Drosophila*. *J Cell Biol* **201**, 531–539.
- 38 Takats S, Pircs K, Nagy P, Varga A, Karpati M, Hegedus K, Kramer H, Kovacs AL, Sass M & Juhasz G (2014) Interaction of the HOPS complex with Syntaxin 17 mediates autophagosome clearance in *Drosophila*. *Mol Biol Cell* **25**, 1338–1354.
- 39 Lorincz P, Kenez LA, Toth S, Kiss V, Varga A, Csizmadia T, Simon-Vecsei Z & Juhasz G (2019) Vps8 overexpression inhibits HOPS-dependent trafficking routes by outcompeting Vps41/Lt. *eLife* **8**, e45631.
- 40 Wu Q, Sun X, Yue W, Lu T, Ruan Y, Chen T & Zhang D (2016) RAB18, a protein associated with Warburg Micro syndrome, controls neuronal migration in the developing cerebral cortex. *Mol Brain* **9**, 19.
- 41 Nian FS, Li LL, Cheng CY, Wu PC, Lin YT, Tang CY, Ren BS, Tai CY, Fann MJ, Kao LS *et al.* (2019)

- Rab18 collaborates with Rab7 to modulate lysosomal and autophagy activities in the nervous system: an overlapping mechanism for Warburg micro syndrome and Charcot-Marie-Tooth neuropathy type 2B. *Mol Neurobiol* **56**, 6095–6105.
- 42 Diao J, Liu R, Rong Y, Zhao M, Zhang J, Lai Y, Zhou Q, Wilz LM, Li J, Vivona S *et al.* (2015) ATG14 promotes membrane tethering and fusion of autophagosomes to endolysosomes. *Nature* **520**, 563–566.
- 43 McEwan DG, Popovic D, Gubas A, Terawaki S, Suzuki H, Stadel D, Coxon FP, Miranda de Stegmann D, Bhogaraju S, Maddi K *et al.* (2015) PLEKHM1 regulates autophagosome-lysosome fusion through HOPS complex and LC3/GABARAP proteins. *Mol Cell* **57**, 39–54.
- 44 Lee G, Liang C, Park G, Jang C, Jung JU & Chung J (2011) UVRAG is required for organ rotation by regulating Notch endocytosis in *Drosophila*. *Dev Biol* **356**, 588–597.
- 45 Pulipparacharuvil S, Akbar MA, Ray S, Sevrioukov EA, Haberman AS, Rohrer J & Kramer H (2005) *Drosophila* Vps16A is required for trafficking to lysosomes and biogenesis of pigment granules. *J Cell Sci* **118**, 3663–3673.
- 46 Lorincz P, Lakatos Z, Varga A, Maruzs T, Simon-Vecsei Z, Darula Z, Benko P, Csordas G, Lippai M, Ando I *et al.* (2016) MiniCORVET is a Vps8-containing early endosomal tether in *Drosophila*. *eLife* **5**, e14226.
- 47 Piracs K, Nagy P, Varga A, Venkei Z, Erdi B, Hegedus K & Juhasz G (2012) Advantages and limitations of different p62-based assays for estimating autophagic activity in *Drosophila*. *PLoS ONE* **7**, e44214.
- 48 Takats S, Glatz G, Szenci G, Boda A, Horvath GV, Hegedus K, Kovacs AL & Juhasz G (2018) Non-canonical role of the SNARE protein Ykt6 in autophagosome-lysosome fusion. *PLoS Genet* **14**, e1007359.
- 49 Glatz G, Gogl G, Alexa A & Remenyi A (2013) Structural mechanism for the specific assembly and activation of the extracellular signal regulated kinase 5 (ERK5) module. *J Biol Chem* **288**, 8596–8609.

Supporting information

Additional supporting information may be found online in the Supporting Information section at the end of the article.

Video S1. 3D structure of lysosome chains and tubules in a Rab3GAP-Rab18 module loss-of-function cell. Video was made by 3D rendering of 21 slices (0.1 μm thickness/slice) from a high-magnification Z-stack image taken from a Rab3GAP1 RNAi cell clone (compressed image shown on Fig. 5C).